2019

Summer Carbonate Chemistry in the Dalton Polynya, East Antarctica

MC Arroyo
Virginia Institute of Marine Science

EH Shadwick
Virginia Institute of Marine Science

B Tilbrook

JGR Oceans

RESEARCH ARTICLE
10.1029/2018JC014882

Summer Carbonate Chemistry in the Dalton Polynya, East Antarctica

M. C. Arroyo[1], E. H. Shadwick[1,2,3], and B. Tilbrook[2,3]

[1]Virginia Institute of Marine Science, William & Mary, Gloucester Point, Virginia, USA, [2]CSIRO Oceans and Atmosphere, Hobart, Tasmania, Australia, [3]Antarctic Climate & Ecosystems Cooperative Research Centre, Hobart, Tasmania, Australia

Key Points:

- The Dalton Polynya was a weak net source of CO_2 to the atmosphere during summer observations
- Net community production estimates were 5-20 mmol C m^{-2} day^{-1} in ice-free and -4-0 mmol C m^{-2} day^{-1} in ice-covered regions
- Remotely sensed products reveal below average surface chlorophyll *a* and above average sea ice cover in contrast to long-term summer means

Correspondence to:
M. C. Arroyo,
marroyo@vims.edu

Citation:
Arroyo, M. C., Shadwick, E. H., & Tilbrook, B. (2019). Summer carbonate chemistry in the Dalton Polynya, East Antarctica. *Journal of Geophysical Research: Oceans*, *124*. https://doi.org/10.1029/2018JC014882

Received 20 DEC 2018
Accepted 15 JUL 2019
Accepted article online 23 JUL 2019

Abstract The carbonate chemistry in the Dalton Polynya in East Antarctica (115°–123°E) was investigated in summer 2014/2015 using high-frequency underway measurements of CO_2 fugacity (fCO_2) and discrete water column measurements of total dissolved inorganic carbon (TCO_2) and total alkalinity. Air-sea CO_2 fluxes indicate this region was a weak net source of CO_2 to the atmosphere (0.7 ± 0.9 mmol C m^{-2} day^{-1}) during the period of observation, with the largest degree of surface water supersaturation ($\Delta fCO_2 = +45$ μatm) in ice-covered waters near the Totten Ice Shelf (TIS) as compared to the ice-free surface waters in the Dalton Polynya. The seasonal depletion of mixed-layer TCO_2 (6 to 51 μmol/kg) in ice-free regions was primarily driven by sea ice melt and biological CO_2 uptake. Estimates of net community production (NCP) reveal net autotrophy in the ice-free Dalton Polynya (NCP = 5–20 mmol C m^{-2} day^{-1}) and weakly heterotrophic waters near the ice-covered TIS (NCP = −4–0 mmol C m^{-2} day^{-1}). Satellite-derived estimates of chlorophyll *a* (Chl *a*) and sea ice coverage suggest that the early summer season in 2014/2015 was anomalous relative to the long-term (1997–2017) record, with lower surface Chl *a* concentrations and a greater degree of sea ice cover during the period of observation; the implications for seasonal primary production and air-sea CO_2 exchange are discussed. This study highlights the importance of both physical and biological processes in controlling air-sea CO_2 fluxes and the significant interannual variability of the CO_2 system in Antarctic coastal regions.

Plain Language Summary Coastal polynyas in Antarctica are dynamic regions that play important roles in the global cycling of carbon. Polynyas are reoccurring areas of open water within sea ice and are often associated with enhanced rates of photosynthesis and exchange of carbon dioxide between the atmosphere and ocean surface. In this study, we use shipboard observations from the first oceanographic cruise in the Dalton Polynya near the Totten and Moscow University Ice Shelves in East Antarctica to characterize the inorganic carbon chemistry in the summertime. We find that the surface concentrations of total dissolved inorganic carbon are reduced in areas of open water mainly as a result of seasonal sea ice melt and the uptake of inorganic carbon by photosynthesis and less so due to air-sea exchange of carbon dioxide. Compared to other coastal polynyas in East Antarctica, our results show that the Dalton Polynya may have smaller rates of net photosynthesis and carbon dioxide exchange.

1. Introduction

The Southern Ocean plays an integral part in the global biogeochemical cycling of carbon, mediating the exchange of both natural and anthropogenic CO_2 between the upper ocean and atmosphere (Arrigo, van Dijken, & Long, 2008; Sabine et al., 2004; Takahashi et al., 2009). Although several global estimates of air-sea CO_2 exchange agree that the open Southern Ocean sustains one of the largest sinks of atmospheric CO_2 (Gruber et al., 2009; Khatiwala et al., 2009; Lenton et al., 2013), uncertainties remain regarding the magnitude of this CO_2 uptake along Antarctic continental shelves that are seasonally covered with sea ice (Lenton et al., 2013). Models are confounded in these regions by the limited number of direct observations and significant natural variability of the CO_2 system on both temporal and spatial scales (e.g., McNeil et al., 2011).

Polynyas are reoccurring areas of open water surrounded by sea ice that form along the coasts of the Antarctic icescape, typically in the lee of a fixed boundary, such as a grounded iceberg or a glacial tongue. In these regions, strong ocean currents and/or katabatic winds push newly formed sea ice away to sustain areas of open water or thin ice for much of the year (Massom et al., 1998; Morales Maqueda et al., 2004).

There is a growing understanding of the interactive physical and biological processes impacting CO_2 system dynamics in seasonally sea ice-covered regions such as the East Antarctic (Roden et al., 2016; Shadwick et al., 2014), the West Antarctic Peninsula (Jones et al., 2017; Legge et al., 2017), and the Amundsen (Mu et al., 2014; Yager et al., 2016) and Ross Seas (DeJong et al., 2015; DeJong & Dunbar, 2017). In the spring and summer, coastal polynyas often support intense biological activity relative to their small surface areas as reduced sea ice coverage exposes surface waters to incoming solar radiation (Arrigo & van Dijken, 2003), driving a dramatic undersaturation in CO_2 at the ocean surface. The timing and magnitude of surface biological CO_2 drawdown are strongly influenced by local sea ice dynamics that determine light and micronutrient (e.g., iron) availability, water column stratification, and the degree of open water. The organic matter that forms during the productive season can be recycled in the mixed layer or exported to depth where it will be subsequently remineralized back to CO_2. In winter, deep convective mixing driven by brine rejection during sea ice formation reinjects CO_2-rich waters to the surface layer where the presence of sea ice may act as a barrier for air-sea exchange and prevent the outgassing of CO_2 to the atmosphere (Loose et al., 2011; Yager et al., 1995). In some Antarctic polynyas, these CO_2-rich waters may additionally be transported off the continental shelf with the formation of dense water (Shadwick et al., 2014). Their disproportionate roles in the air-sea exchange of CO_2 (e.g., Sweeney, 2003), primary production (e.g., Shadwick et al., 2017), and in some cases Dense Shelf Water and Antarctic Bottom Water formation (Orsi et al., 1999; Rintoul, 1998; Williams et al., 2008) make these coastal polynya systems important players in the biogeochemical cycles of the Southern Ocean.

Despite the importance of the continental shelf regions in global carbon cycling, few observational CO_2 system studies have been conducted in the coastal East Antarctic. The Dalton Polynya is a coastal polynya located on the Sabrina Coast in East Antarctica, forming in the lee of the Dalton Iceberg Tongue (Figure 1). The surrounding Totten and Moscow University Ice Shelves (TIS and MUIS, respectively), which terminate at the sea boundary in the Dalton Polynya, are among the fastest thinning on the East Antarctic Ice Sheet, with high rates of mass loss (Mohajerani et al., 2018) and basal ice shelf melting near their grounding lines over the past 15 years (Rignot et al., 2013). Basal melting of these ice shelves is driven by on shelf intrusions of relatively warm (>0 °C) modified Circumpolar Deep Water to ice shelf cavities (Li et al., 2015; Rintoul et al., 2016; Silvano et al., 2017) and is modulated by surface winds stress (Greene et al., 2017). These high basal melt rates (>4 m/year) are similar to those observed in the West Antarctic Ice Sheet near the Amundsen and Bellingshausen Seas, regions often thought of as more vulnerable to mass loss and glacial thinning (Rignot et al., 2013; Silvano et al., 2017). Meltwater input to the Dalton Polynya contributes to significant water column freshening, reducing the possibility for dense water formation in the region (Silvano et al., 2018). Previous studies in the coastal Antarctic suggest glacially derived meltwater may influence mixed-layer biogeochemistry and carbon cycling by stimulating high levels of primary production through the delivery of iron and other essential micronutrients to surface waters (e.g., Eveleth et al., 2017, Gerringa et al., 2012). The potential impacts of glacial mass loss and high rates of basal melting to the Dalton Polynya system may drive future changes in biological production and air-sea CO_2 flux that ultimately influence the carbonate chemistry.

Here we present CO_2 system measurements from the Dalton Polynya in early summer (Figure 1). A combination of high-frequency underway measurements of sea surface CO_2 fugacity (fCO_2) along the ship track and discrete samples of total dissolved inorganic carbon (TCO_2) and total alkalinity (TA) is used to characterize the biogeochemistry of the region. The physical and biological processes responsible for observed distributions of mixed-layer TCO_2 are examined, and net community production is computed via seasonal deficits in TCO_2 concentration. Additionally, the spatial variability of air-sea CO_2 fluxes is evaluated. These new observations are also examined in comparison to the long-term (1997–2017) surface chlorophyll *a* concentration and sea ice coverage derived from remote sensing products to assess interannual variability. Results from the Dalton Polynya highlight the importance of both physical and biological processes in controlling the significant seasonality in the CO_2 system of Antarctic coastal waters.

2. Oceanographic Setting

We follow the water mass characterization of Silvano et al. (2017) to define the four major water masses in the Dalton Polynya (DP) during the summer season, constrained here by potential density anomaly surfaces

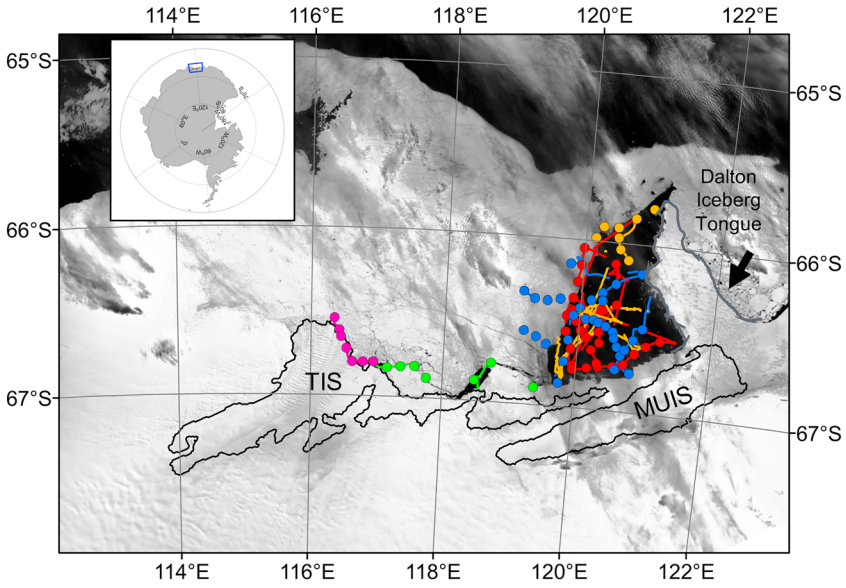

Figure 1. Map of the Dalton Polynya. Underway ship track (lines) and CTD stations (circles) on the *RV Aurora Australis* between 24 December 2014 and 8 January 2015 overlain on a MODIS-Terra satellite image from 10 January 2015. Observations were made within the polynya and near both the Moscow University Ice Shelf (MUIS) and the Totten Ice Shelf (TIS). Red indicates measurements between 24 and 29 December 2014 (DP1). Blue indicates measurements between 2 and 5 January 2015 and three CTD stations on 7 January (DP2). Yellow indicates measurements between 6 and 8 January 2015 (DP3). Measurements made near the TIS are indicated in magenta (West Totten; WT) and green (East Totten; ET) between 30 December 2014 and 1 January 2015.

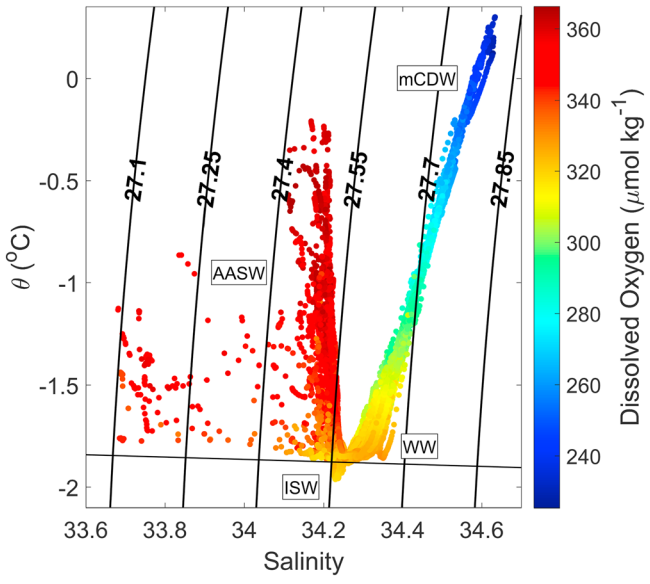

Figure 2. Potential temperature (θ; °C) and salinity diagram, with contours of potential density anomaly (σ_θ; kg/m^3), and colors for dissolved oxygen (μmol/kg). The black thick solid line marks the surface freezing point of seawater. Water masses are labeled as Antarctic Surface Water (AASW), modified Circumpolar Deep Water (mCDW), Winter Water (WW), and Ice Shelf Water (ISW). See text and Table 1 for definitions.

referenced to surface pressure (σ_θ, kg/m^3) and potential temperature (θ, °C; Figure 2 and Table 1). Antarctic Surface Water (AASW) is the lightest ($\sigma_\theta < 27.55$ kg/m^3) and is highly variable in surface temperature (between −1.86 and −0.23 °C) and salinity (between 33.6 and 34.2; Figure 2). AASW is relatively fresh, due to seasonal melting from both the surrounding sea ice and the ice shelves to the south. This water mass varies in thickness across the region: in the ice-free DP, AASW occupies the upper ~80 m (Figure 3); near the TIS, signals of AASW virtually disappear, as Winter Water (WW) reaches the surface (Figure 4). WW ranges between $27.55 < \sigma_\theta < 27.70$ kg/m^3 and $-1.92 < \theta < -1.75$ °C and occupies most of the water column in summer as a product of vertical convection. The depth range of WW depends on its location within the polynya, as WW shoals nearly to the surface along the ice shelves.

Dense Shelf Water does not form in the DP. Instead, relatively warm, salty modified Circumpolar Deep Water (mCDW) floods the deep basin in summer ($\sigma_\theta > 27.70$ kg/m^3), bringing heat, nutrient, CO_2-rich, and relatively O_2-poor water onto the shelf. The inflow of mCDW through deep troughs in both the TIS and MUIS delivers a substantial amount of heat to drive rapid basal melt at the grounding line (Greenbaum et al., 2015; Rintoul et al., 2016; Silvano et al., 2017). At the MUIS ice front, the melting drives the formation of Ice Shelf Water (ISW), through the mixture of basal ice shelf meltwater and WW. ISW is supercooled due to pressure at $\theta < -1.92$ °C within the same σ_θ range as WW. The input of basal meltwater, particularly near the MUIS, also leads to a shoreward freshening of WW near the southern edge of the DP (Silvano et al., 2017).

Table 1
Water Mass Classifications

Water mass	σ_θ (kg/m^3)	θ (°C)
Antarctic Surface Water	$\sigma_\theta < 27.55$	
Winter Water	$27.55 < \sigma_\theta < 27.7$	$-1.92 < \theta < -1.75$
Ice Shelf Water	$27.55 < \sigma_\theta < 27.7$	$\theta < -1.92$
Modified Circumpolar Deep Water	$27.7 < \sigma_\theta$	

Note. Constraints of potential density anomaly (σ_θ; kg/m^3) and potential temperature (θ; °C) follow definitions by Silvano et al. (2017).

3. Methods

Observations were made during a survey of the Dalton Polynya and surrounding ice shelves along the Sabrina Coast (116°–122°E) on board the *RV Aurora Australis* between 25 December 2014 and 8 January 2015 (Figure 1; Rosenberg & Rinoul, 2016). The ship occupied 68 stations in the DP and near the MUIS and 13 stations in a lead in front of the TIS. During each cast, continuous measurements of temperature (°C), salinity, pressure (dbar), and dissolved oxygen (μmol/kg) were made using SeaBird instruments (SBE9plus and SBE43 models). Instruments were mounted onto a rosette frame with 22 10-L General Oceanics Niskin bottles for discrete seawater sampling; hydrographic property analysis of conductivity, temperature, and depth (CTD) data is described further in Silvano et al. (2017).

The shelf can be separated into two broad regions: DP refers to the region east of 119°E and TIS refers to the region west of 119°E. These regions are further partitioned into subregions illustrated in Figure 1. The DP includes measurements made between 24 and 29 December (DP1, blue), between 2 and 5 January and three CTD stations on 7 January (DP2, red), and between 6 and 8 January (DP3; yellow). The TIS region includes measurements between 30 December and 1 January and is divided into West Totten (WT; magenta) and East Totten (ET; green).

3.1. Discrete CO_2 System and Biogeochemical Observations

Discrete samples of TCO_2 and TA were collected into 250-ml bottles at each station. Each sample was immediately fixed with a saturated solution of mercuric chloride to halt biological activity. TCO_2 and TA concentrations were measured on board by coulometric titration using a Single Operator Multiparameter Metabolic Analyzer (SOMMA) system and by automatic open-cell potentiometric titration with 0.1 M hydrochloric acid, respectively, following methods of Dickson et al. (2007). Routine analysis of Certified Reference Material (CRM Batch #137) from A. G. Dickson ensured that the analytical uncertainties (precision and accuracy) were better than ±1.4 μmol/kg for TCO_2 and ±1.5 μmol/kg for TA.

Samples of dissolved oxygen were collected in parallel to CO_2 system observations and analyzed on board by Winkler Titration following methods of Hood et al. (2010), with an uncertainty of <1%. Inorganic nutrient samples were collected for phosphate (PO_4^{-3}) and silicic acid ($Si(OH)_4$) and frozen until analysis at CSIRO in Hobart, Australia, following standard methods of Grasshoff et al. (2007). Uncertainties for PO_4^{-3} and $Si(OH)_4$ were <5%.

The saturation state of aragonite (Ω_{Ar}) and pH on the total scale were calculated from TCO_2 and TA using CO_2SYS program by van Heuven et al. (2011), using the thermodynamic equilibrium constants by Mehrbach et al. (1973) refit by Dickson and Millero (1987). Average values of PO_4^{-3} (2.06 ± 0.07 μmol/kg) and $Si(OH)_4$ (64 ± 7 μmol/kg) were used. Calcium ion concentration was assumed to be conservative with and calculated from salinity (Riley & Tongudai, 1967).

3.2. Underway fCO_2 Measurements and Air-Sea CO_2 Flux Calculations

Continuous high-resolution underway measurements of the fCO_2, sea surface salinity, and sea surface temperature were made from the seawater intake ~4 m below the ocean surface. The fCO_2 in seawater was measured via continuous flow equilibration using a nondispersive infrared spectrometer (LI-COR, LI7000; Pierrot et al., 2009). The underway fCO_2 system was calibrated every 4 hr with four standards: a CO_2-free air and three CO_2 concentrations of 299.41, 354.00, and 402.15 μatm in dry air on the WMO-X2007 mole

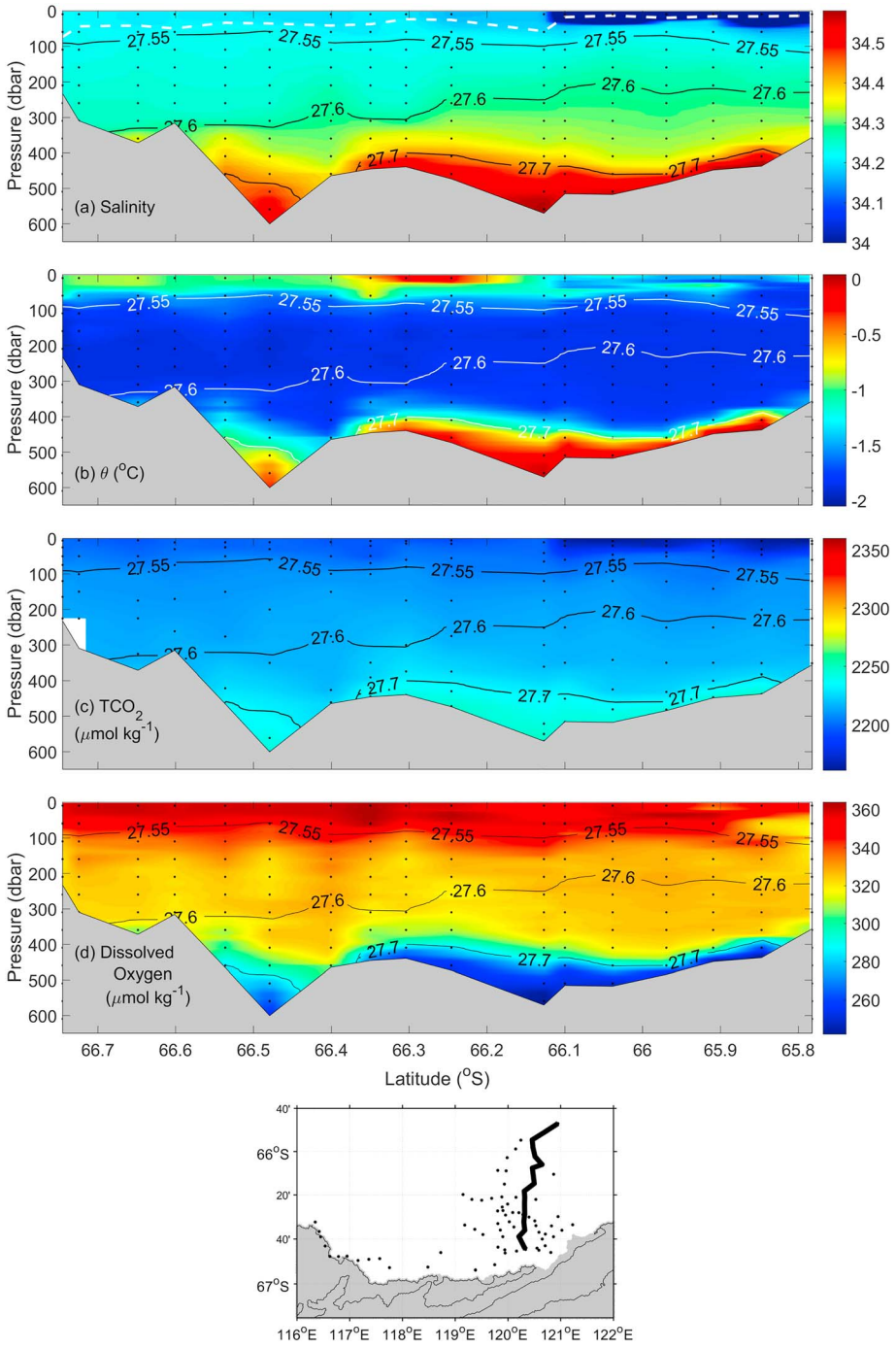

Figure 3. Offshore (north-south) section through the Dalton Polynya for (a) salinity, (b) potential temperature (θ; °C), (c) TCO_2 (μmol/kg), and (d) dissolved oxygen (μmol/kg) with contours of potential density anomaly (kg/m^3) and white dashed contour of calculated mixed layer depth in (a). The black dots indicate the station locations.

fraction scale. Approximately 70 s were needed for the seawater to pass from the ship intake to the CO_2 system, warming by less than 0.6 °C. All fCO_2 measurements were corrected to in situ temperature and salinity and to 100% humidity. The atmospheric mole fraction of CO_2 was also measured at roughly 16 m above sea level to calculate the atmospheric fCO_2. The mean atmospheric fCO_2 was 379 ± 1.7 μatm throughout the voyage. The fCO_2 measurement uncertainties are 2 μatm in seawater and 0.2 μatm in air at 350 μatm.

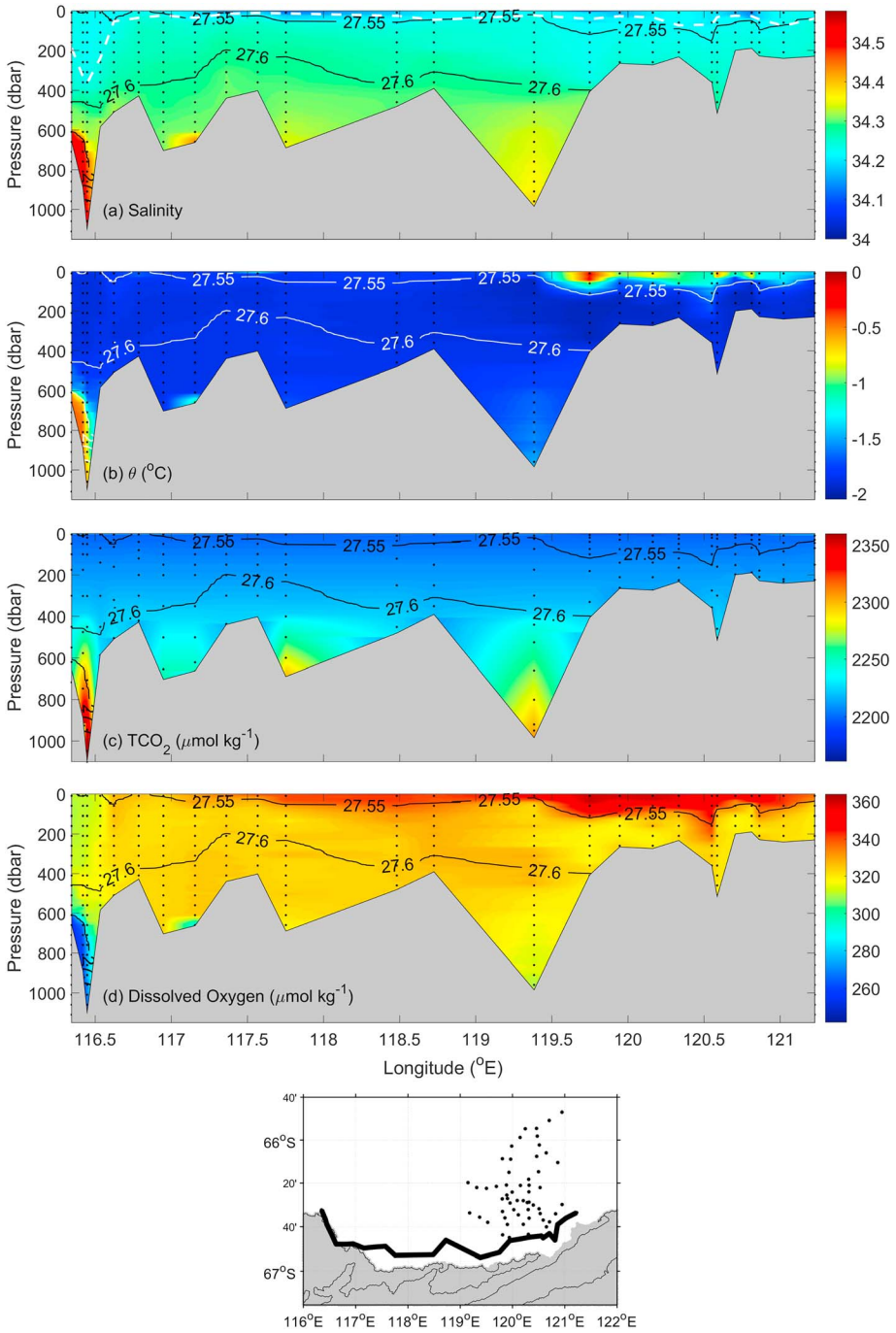

Figure 4. Along-shore (west-east) section in front of the Totten and Moscow University Ice Shelves for (a) salinity, (b) potential temperature (θ; °C), (c) TCO_2 (μmol/kg), and (d) dissolved oxygen (μmol/kg) with contours of potential density anomaly (kg/m^3) and white dashed contour of calculated mixed layer depth in (a). The black dots indicate the station locations.

The air-sea flux of CO_2 between the sea surface and the atmosphere was computed via the following equation:

$$F_{CO2} = k\ \alpha\ \Delta fCO_2 \quad (1)$$

where F_{CO2} is the flux (mmol C m^{-2} day^{-1}), k is the gas transfer velocity, α is the solubility of CO_2 (Weiss, 1974), and ΔfCO_2 (μatm) is the gradient in fCO_2 between the atmosphere and sea surface

($\Delta fCO_2 = fCO_2^{sea} - fCO_2^{air}$). A positive flux indicates a net transfer from the ocean to the atmosphere (i.e., outgassing). The parametrization of Wanninkhof (2014) was used to compute k using daily averaged short-term winds, consistent with methodology from other polynya regions (e.g., Gibson & Trull, 1999; Shadwick et al., 2014, 2017), from the National Centers for Environmental Prediction and National Center for Atmospheric Research (NCEP/NCAR) Reanalysis product recorded at 10-m height above the sea surface (Kalnay et al., 1996). The exchange time of CO_2 between the surface ocean and the atmosphere is on the order of months (Broecker & Peng, 1974) and air-sea CO_2 fluxes were similarly computed using a long-term gas transfer velocity term to provide a broader context for instantaneous (short-term) fluxes. A long-term k was calculated from the average of the daily second moment of the wind speed (<wind speed>^{2}) across eight NCEP/NCAR grid cells (within the spatial range of 65 - 68°S and 116 - 122°E) between December 2014 and January 2015 (Evans et al., 2015; Wanninkhof, et al. 2004). We estimate an uncertainty associated with the air-sea CO_2 flux of 0.3 mmol C m^{-2} day^{-1} by comparing results obtained with several different gas transfer parameterizations (Edson et al., 2011; Ho et al., 2006; Sweeney et al., 2007; Wanninkhof, 1992).

3.3. Seasonal Partitioning of TCO_2 and Net Community Production Computations

Seasonal changes of TCO_2 in the summer mixed layer are influenced both by physical (e.g., air-sea CO_2 exchange, mixing, and calcium carbonate dissolution) and biological (e.g., photosynthesis, respiration, and calcium carbonate formation) processes. The summer mixed layer depth (MLD) at each station is defined here as the depth at which the potential density exceeds that of a reference measurement at 10 m by a threshold 0.01 kg/m^3 (e.g., Shadwick et al., 2014) and was comparable to MLD expressed as the maximum of the buoyancy frequency (Carvalho et al., 2017). Although observed summer MLDs in the DP were typically <100 m, deeper vertical mixing earlier in the productive season (i.e., late winter, early spring) extends well below 100 m (Williams et al., 2011). Late-winter measurements in 2007 found the deepest winter mixed layer on the Sabrina Coast in the northern DP, reaching depths >350 m (Williams et al., 2011). Summer MLDs in front of the western TIS, however, were significantly deeper (MLDs >180 m) than in the open waters of the DP.

Wintertime TCO_2 concentration in surface waters is often estimated using the value at the temperature minimum (e.g., Bates et al., 1998; Roden et al., 2016). However, on the Antarctic shelf, the temperature minimum is not well defined, for example in the areas in front of the MUIS where ISW is present (Silvano et al., 2017). Profiles of TCO_2 indicate a consistent concentration at depths in the WW water mass ($27.55 < \sigma_\theta < 27.70$ kg/m^3 and $-1.92 < \theta < -1.75$ °C), roughly between 150 and 350 m. Thus, we estimate the surface wintertime TCO_2 concentration as the average concentration at 150 m depth ($TCO_2^{winter} = 2{,}216 \pm 2$ μmol/kg, $n = 26$). Measurements of TCO_2 and TA are normalized to the average regional salinity ($S = 34.3$) to account for the seasonal variations in concentration due to changes in salinity from sea ice formation and melting, as well as mixing (e.g., Shadwick et al., 2014).

The seasonal change in TCO_2 due to biological processes is expressed as the net community production (NCP), the difference between net primary production and heterotrophic respiration. NCP (mmol C m^{-2} day^{-1}) was computed at each station by the depth integrated seasonal deficit of salinity normalized TCO_2 ($nTCO_2$) via

$$\mathrm{NCP} = \int_{z=0}^{z=100} [n\mathrm{TCO_2}]^{\mathrm{winter}} - [n\mathrm{TCO_2}]^{\mathrm{observations}}\, \mathrm{d}z \quad (2)$$

where z is depth in meters. Although MLDs at each station were above 100 m within the open waters of the Dalton Polynya, we integrated to 100 m to account for deeper vertical mixing earlier in the productive season (Bates et al., 1998; Shadwick et al., 2014; Williams et al., 2011). The length of the productive season was defined as time since 1 November 2014 based on the increase in surface chlorophyll a (Chl a) concentration relative to winter months (June, July, and August) inferred from Moderate Resolution Imaging Spectroradiometer (MODIS)-Aqua satellite imagery during the 2014/2015 summer season (see section 5.2). This estimation of NCP does not account for the contribution of seasonal air-sea CO_2 exchange, although the contribution is small based on summer F_{CO2} computations (see sections 4.2 and 5.1 for further discussion).

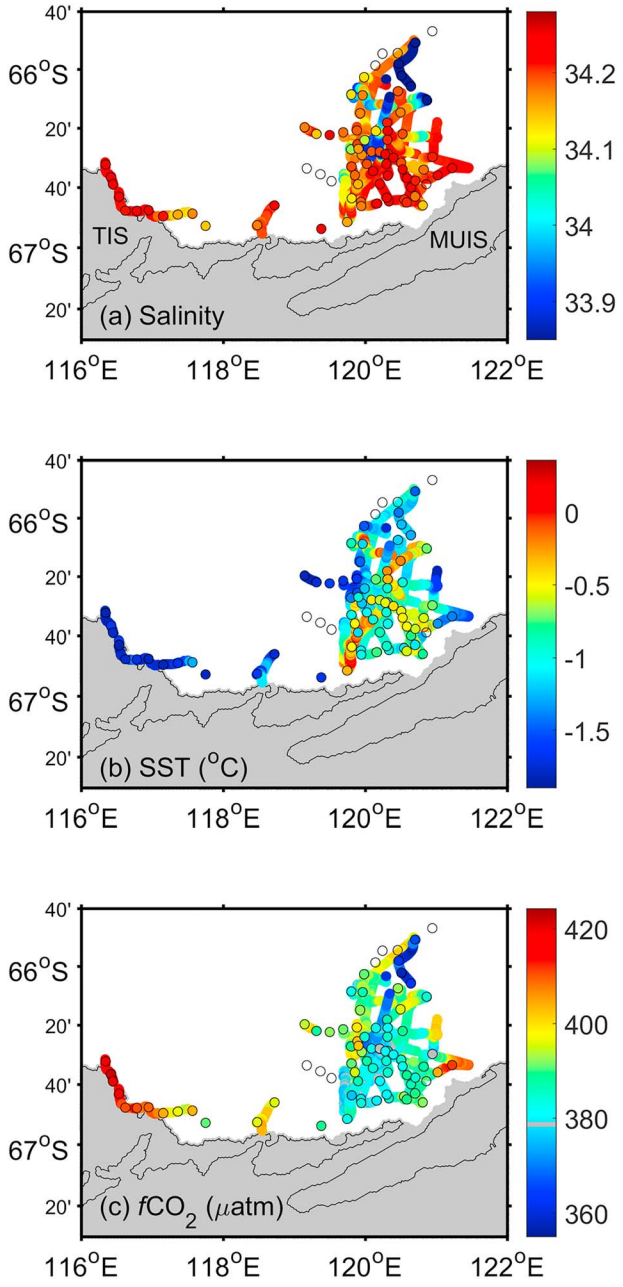

Figure 5. Underway surface measurements in the Dalton Polynya for (a) salinity, (b) sea surface temperature (SST; °C), and (c) fCO_2 (μatm). The mean atmospheric fCO_2 (379 μatm) is indicated by the gray line in the color bar of (c). Colored circles correspond to the underway measurements taken at the time of CTD sampling. TIS = Totten Ice Shelf; MUIS = Moscow University Ice Shelf.

3.4. Satellite Remote Sensing Products

Satellite-derived sea surface Chl *a* concentrations were obtained from Level 3 processed, 9-km resolution measurements from SeaWiFS (Sea-viewing Wide Field-of-view Sensor) between July 1997 and June 2002 and from MODIS-Aqua between July 2002 and June 2017. Similarly, sea ice coverage estimates were obtained from the Special Sensor Microwave/Imager (SMM/I) and the Special Sensor Microwave Imager/Sounder (SMMIS) on the Defense Meteorological Satellite Program (DMSP) satellite from the National Snow and Ice Data Center (NSIDC) between July 1997 and June 2017 at 25-km resolution and Level 3 processing. All data presented here are monthly averaged values in the Dalton Polynya, within the region between 65.8 and 67.0°S and 119 and 121°E (see Figure 1).

4. Results

4.1. Hydrographic and Biogeochemical Properties

AASW (σ_θ < 27.55 kg/m^3) in the DP was relatively warm and fresh, reflecting the summer conditions of surface warming and local sea ice melt (Figures 2 and 5 and Table 2). Sea surface salinity was between about 33.9 and 34.3 within the DP (east of 119°E). In the northern DP, minimum surface salinity (S < 33.9) was observed toward the end of the voyage, likely driven by melting sea near the Dalton Iceberg Tongue. Sea surface temperatures were warmer in the central DP with values ranging from −1.2 to +0.4 °C, and colder near the outer edges of the polynya and near the TIS with a minimum of −1.8 °C (Figure 5b). In front of the TIS, WW outcropped to the surface, and salinities of ~34.25 were observed.

The mean concentration of dissolved oxygen (~341 μmol/kg) in AASW was greater than values found elsewhere in East Antarctica (Roden et al., 2016; Shadwick et al., 2014), with concentrations more comparable to saturated conditions (~350–360 μmol/kg) though similar surface temperature and salinity was observed (Table 2). The percent saturation of dissolved oxygen at the sea surface was greatest (>99%) in the central, open waters of the Dalton Polynya (Figure 3d) and decreased toward and along the outer edges of the polynya and near the TIS (Figure 4d). In front of the TIS, surface dissolved oxygen reached a minimum concentration (305 μmol/kg, 85% saturation), coincident with the WW outcrop and entrainment of oxygen-poor subsurface waters. Dissolved oxygen concentration further decreased with depth below the surface mixed layer in WW (Figures 3d and 4d) to values ranging between 300 and 330 μmol/kg, signaling the biological imprint of dissolved oxygen consumption. The cumulative influence of the remineralization of organic matter over longer time scales (i.e., years) is seen more dramatically in mCDW, where dissolved oxygen reaches as low as 220 μmol/kg due to its isolation from the atmosphere.

4.2. Underway fCO_2 and Air-Sea CO_2 Exchange

The surface and mixed layer distribution of dissolved oxygen spatially mirrors the trends in underway fCO_2 (Figures 3d, 4d, and 5c), where the lowest concentrations of dissolved oxygen are found in areas of high fCO_2. The sea surface fCO_2 indicates that the region was mostly supersaturated or near equilibrium with respect to the average atmospheric value (379 μatm; Figures 5c and 6a) in both the DP and near the TIS. There was a distinct difference in surface fCO_2 in areas with the absence (within DP) or presence (near TIS) of sea ice. In areas of open water in the DP, fCO_2 ranged from 370 to 405 μatm, extending to a

Table 2
Characteristic Mean Values of Potential Density Anomaly (σ_θ; kg/m^3), Potential Temperature (θ; °C), Salinity (S), Dissolved Oxygen (O_2; µmol/kg), Total Dissolved Inorganic Carbon (TCO_2; µmol/kg), Total Alkalinity (TA; µmol/kg), pH, and Aragonite Saturation State (Ω_{Ar}) of Each Water Mass in the Dalton Polynya Region of East Antarctica

Parameter	AASW	WW	ISW	mCDW
σ_θ	27.48	27.59	27.56	27.74
θ	−1.24	−1.84	−1.94	−0.36
S	34.17	34.27	34.24	34.53
O_2	341	316	311	251
TCO_2	2,200	2,215	2,214	2,242
TA	2,310	2,315	2,313	2,335
pH	8.04	8.01	8.01	7.94
Ω_{Ar}	1.30	1.17	1.17	1.03

maximum of 410 µatm near the eastern MUIS. The largest fCO_2 values were recorded near the TIS, with a maximum of 424 µatm at the western edge, exhibiting the correspondingly greatest degree of supersaturation relative to the atmosphere ($\Delta fCO_2 = +45$ µatm). In contrast, the northern DP showed the greatest degree of undersaturation with respect to the atmosphere ($\Delta fCO_2 = -20$ µatm).

The Dalton Polynya was a net source of CO_2 to the atmosphere during the sampling period as determined by both the long-term and instantaneous air-sea CO_2 fluxes with means and standard deviations of 0.5 ± 0.6 mmol C m^{-2} day^{-1} and 0.7 ± 0.9 mmol C m^{-2} day^{-1}, respectively. F_{CO2} values evaluated with a long-term k value reached a maximum of 2.3 mmol C m^{-2} day^{-1} in the most supersaturated waters near the TIS and a minimum of −1.1 mmol C m^{-2} day^{-1} in the northern DP (DP3). Using short-term winds, values of instantaneous F_{CO2} had a larger range, between a maximum surface uptake of 1.0 mmol C m^{-2} day^{-1} to a maximum surface outgassing of 5.1 mmol C m^{-2} day^{-1} from within the center of the DP (DP2) during the study period. Short-term wind speeds were locally variable throughout, ranging between near 0 to 10 m/s (Figure 6b); these fluctuations imposed a correspondingly large variation in flux. In particular, during periods of enhanced wind, defined here as wind speed >8 m/s, and conditions with large ΔfCO_2, there were correspondingly large fluxes of CO_2 (Figure 6, shaded). We observed three high wind events: one at the beginning and two near the end of the study. In the first high wind event, the relatively large ΔfCO_2 resulted in an outgassing of roughly 4.3 mmol C m^{-2} day^{-1}. During

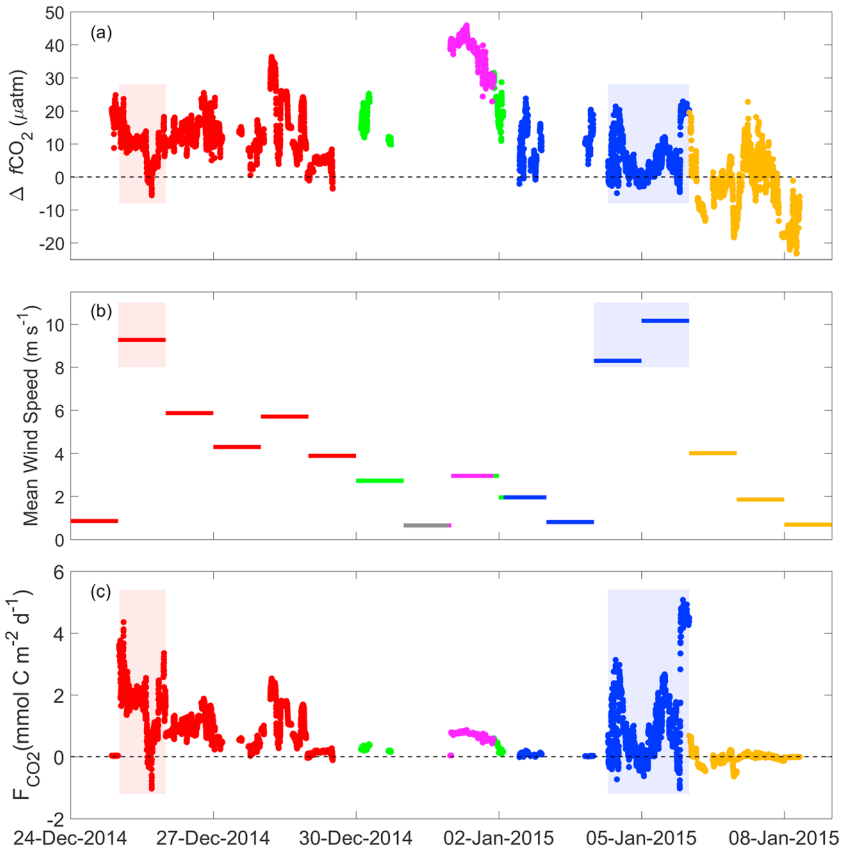

Figure 6. Underway measurements as a function of time between 24 December 2014 and 9 January 2015. (a) ΔfCO_2 (µatm); (b) daily mean wind speed (m/s). Wind speeds >8 m/s are defined as high wind events and are indicated by the red shading in DP1 and blue shading in DP2. (c) Instantaneous F_{CO2} (mmol C m^{-2} day^{-1}) where a positive flux indicates a net ocean source of CO_2. See Figure 1 for color references.

the second high wind event in the DP, a maximum F_{CO_2} of 5.1 mmol C m^{-2} day^{-1} was observed. Although both minimum and maximum ΔfCO_2 values were recorded near the northern DP and TIS, respectively, these gradients were observed during periods of much lower wind speeds (~1 to 3 m/s) and were associated with correspondingly weaker CO_2 fluxes on the order of ~0.02 mmol C m^{-2} day^{-1}.

4.3. CO_2 System Properties in the Dalton Polynya

Vertical profiles of TCO_2 and TA from stations in the DP during each sampling period (DP1, DP2, and DP3) were similar, reflecting the different properties within each water mass (Figure 7). Surface TCO_2 concentrations ranged between 2,190 and 2,211 μmol/kg in the central DP. Minimum surface TCO_2 concentrations (~2,170 μmol/kg) were found in the northern polynya (yellow; DP3), corresponding with the surface salinity minimum. Similarly, surface TA values ranged between 2,303 and 2,314 μmol/kg in the central DP, with a similar feature of minimum values of ~2,276 μmol/kg found in the northern DP. Subsurface parameters converge at a depth of approximately 150 m to an average TCO_2 concentration of 2,214 ± 3 μmol/kg and TA concentration of 2,315 ± 2 μmol/kg in WW (Figures 7a and 7b), similar to other observations made in shelf waters in the East Antarctic (Table 2; Shadwick et al., 2014; Roden et al., 2016).

Profiles of pH and Ω_{Ar} exhibit similar patterns with depth, reflecting the changes in TCO_2 and TA concentrations. The surface pH and Ω_{Ar} were elevated relative to subsurface values, enhanced by the biological drawdown of TCO_2 by photosynthesis. We observed pH values ranging from 8.01 to 8.07 at the surface. Surface Ω_{Ar} ranged from 1.22 and 1.38, with lower values near the western ice edge in the DP (not shown) coincident with regions of elevated surface TCO_2. Ω_{Ar} was supersaturated throughout most of the water column, although undersaturated values of Ω_{Ar} (i.e., $\Omega_{Ar} < 1$) were found at depth in the TCO_2-rich mCDW layer. Below ~400 m, TCO_2 and TA continued to increase while pH and Ω_{Ar} decrease with depth in the mCDW water mass.

The precipitation of calcium carbonate (ikaite) during sea ice formation in the previous autumn and winter season may influence the TCO_2 to TA ratio in both the newly formed sea ice and the underlying seawater (Dieckmann et al., 2008; Jones et al., 2010; Rysgaard et al., 2012; Shadwick et al., 2017). However, from our observations the conservative behaviors of the TA-salinity and the nTA-$nTCO_2$ relationships (Figure 7d inset) suggests that ikaite formation is not a dominant process in the Dalton Polynya.

Salinity-normalizing TCO_2 and TA values accounts for the freshwater dilution of sea ice melt in the Dalton Polynya on surface concentrations; surface to subsurface gradients in $nTCO_2$ and nTA are thus much weaker than in the in-situ observations (Figures 7c and 7d). Surface $nTCO_2$ values ranged between 2,200 and 2,216 μmol/kg and surface nTA to between 2,315 and 2,323 μmol/kg. Higher surface $nTCO_2$ values were found along the western sea ice edges in the DP as compared to the center of the DP (not shown). At 150 m depth, mean $nTCO_2$ concentration was 2,216 ± 2 μmol/kg, which is assumed to represent the winter concentration of $nTCO_2$ at the surface (see section 3.3).

4.4. CO_2 System Properties Near the Totten Ice Shelf

Profiles of CO_2 system parameters show somewhat different properties near the TIS than those described above (Figure 8). Here, WW outcrops to the surface near the TIS, particularly in the western edge (see Figure 4) where MLDs extended over 360 m. The stations occupied in the east TIS (magenta) show a similar pattern with depth as those in the DP, where AASW is present at the surface and MLDs ranged between 12 and 46 m. Surface TCO_2 in the eastern TIS stations show a mean value of 2,205 μmol/kg, similar to the DP, whereas surface TCO_2 in the western TIS show higher values with an average of 2,213 μmol/kg (Figure 8a). Surface $nTCO_2$ was more depleted in the east (~2,212 μmol/kg) than in the west (~2,218 μmol/kg). In WW, the $nTCO_2$ in stations near the TIS converged to 2,217 ± 2 μmol/kg. In stations in the western TIS, $nTCO_2$ at the surface was modestly elevated (between 0 and 4 μmol/kg) relative to the subsurface winter value.

Mean surface pH (~8.02) and Ω_{Ar} (~1.24) near the TIS were lower as compared to the DP. Surface pH and Ω_{Ar} values also increased from west to east spatially in front of the TIS, corresponding to higher concentration of TCO_2 in the west. Ω_{Ar} reached undersaturation ($\Omega_{Ar} < 1$) at depths >750 m.

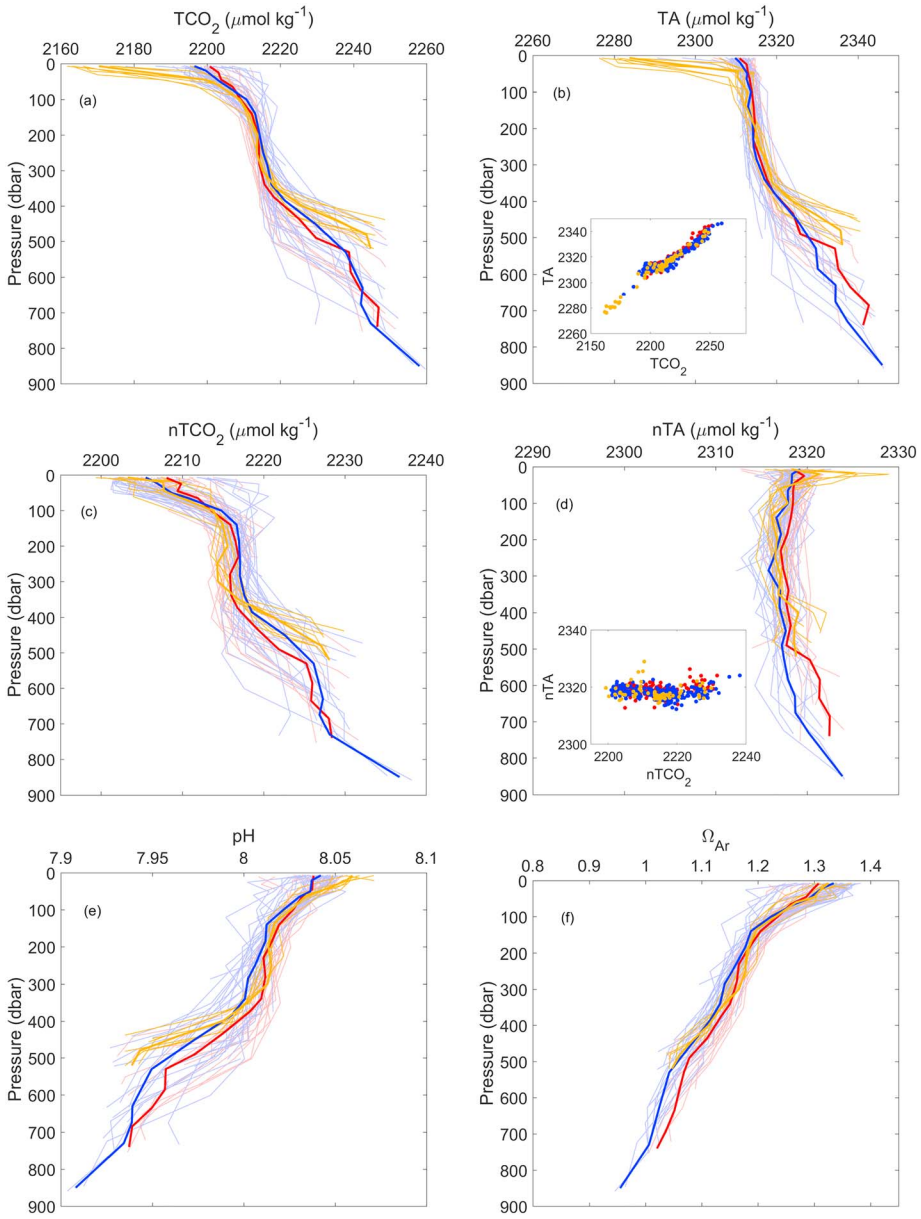

Figure 7. Profiles of CO_2 system properties in the Dalton Polynya. (a) TCO_2 (μmol/kg), (b) TA (μmol/kg) with TA versus TCO_2 inset, (c) $nTCO_2$ (μmol/kg), (d) nTA (μmol/kg) with nTA vs. $nTCO_2$ inset, (e) pH, and (f) saturation state of aragonite (Ω_{Ar}). Bin-averaged profiles are indicated in each with a bold line.

5. Discussion

5.1. Net Community Production

Seasonal depletions of TCO_2 in the upper 100 m were determined and attributed to a combination of physical and biological processes in both waters in the ice-free DP and ice-covered TIS (Figure 9 and Table 3). Processes such as sea ice melt (formation), CO_2 outgassing (ingassing) and photosynthesis (respiration) will decrease (increase) the concentration of TCO_2. Total integrated deficits of TCO_2 (ΔTCO_2^{total}; Table 3) were larger in ice-free regions as compared to areas with greater sea ice coverage. In the DP, the contribution from the seasonal melting of sea ice accounted for less than half of the total change in TCO_2 in DP1 and DP2 but was more significant in DP3. Observations of surface salinity and temperature in DP3 suggest that sea ice melt was ongoing near the Dalton Iceberg Tongue (section 4.1). At all stations in the Dalton Polynya, NCP was positive, ranging between 1 and 21 mmol C m^{-2} day^{-1} (Figure 10a; see section 3.3), indicating

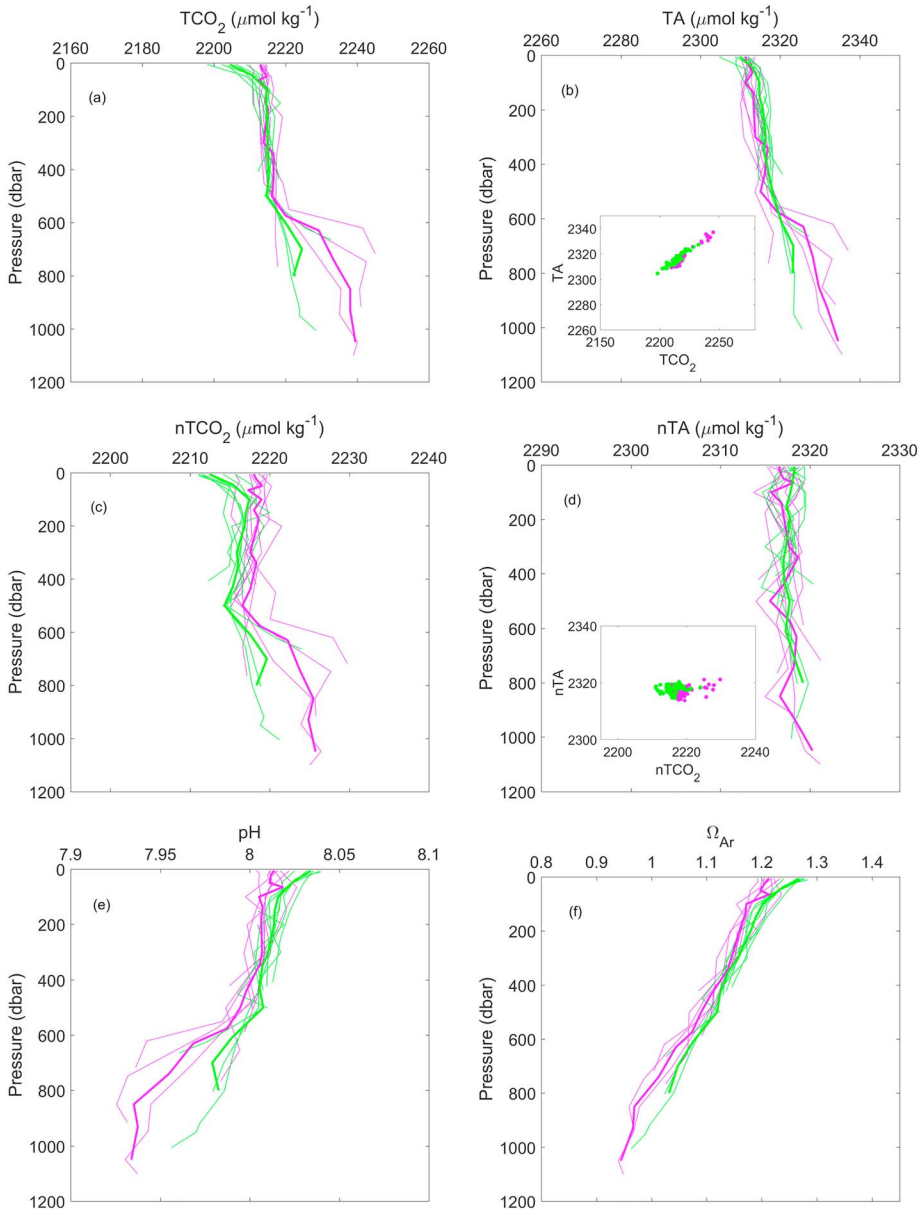

Figure 8. Profiles of CO_2 system properties in front of the Totten Ice Shelf. (a) TCO_2 (μmol/kg), (b) TA (μmol/kg) with TA versus TCO_2 inset, (c) $nTCO_2$ (μmol/kg), (d) nTA (μmol/kg) with nTA versus $nTCO_2$ inset, (e) pH, and (f) saturation state of aragonite (Ω_{Ar}). Binned-averaged values are indicated in each with a bold line.

net autotrophy or the dominance of primary production over respiration (Table 3). Both the $nTCO_2$ deficits and the resulting NCP values were greatest in the center of the DP and lower near the western boundary and the sea ice edge. Estimates of NCP are on the order of 10 to 20 mmol C m^{-2} day^{-1} within the ice-free regions in the polynya and increase over the duration of the of the cruise, from DP1 to DP3, in parallel with decreasing mixed layer $nTCO_2$ concentrations (Figure 10). In the northernmost stations of the polynya (DP3), sea ice melt locally enhanced stratification and stabilized the mixed layer (MLDs = ~12 m), increasing light availability and contributing to enhanced biological activity and greater NCP. This is consistent with observations of decreased fCO_2 in the region (Figure 4a). By contrast, the $nTCO_2$ deficits and NCP are lower in front of the TIS (Table 3), ranging from −3.8 to a maximum of 6.6 mmol C m^{-2} day^{-1}, increasing spatially from west to east in parallel to decreasing MLDs and the increasing dominance of AASW at the surface (Figure 4). In the eastern edge of the TIS (ET), deficits of TCO_2 are dominated by changes in salinity with smaller contributions from biological CO_2 uptake resulting in weakly autotrophic

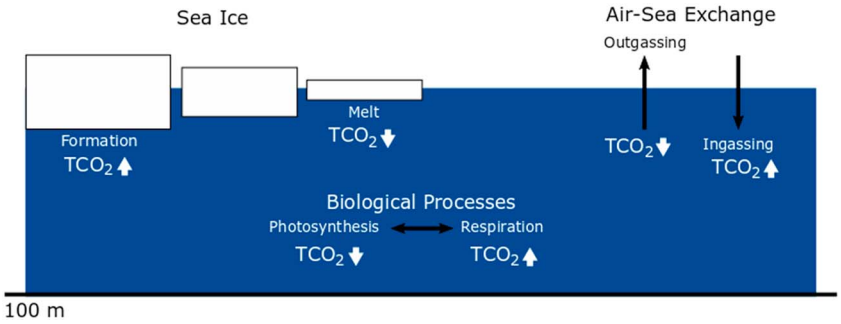

Figure 9. Schematic representing the physical and biological processes driving the changes in TCO_2 concentration in the upper 100 m from the transition from winter to summer in the Dalton Polynya. Physical processes such as sea ice formation and ingassing of atmospheric CO_2 increase TCO_2 concentrations while sea ice melt and outgassing of CO_2 decrease TCO_2 concentrations. Biological photosynthesis reduces TCO_2 concentration through the formation of organic matter, while respiration and the remineralization of this organic matter increases TCO_2 concentration.

conditions. At stations of the western TIS (WT), NCP was negative ranging from −3.8 to 0 mmol C m^{-2} day^{-1}, suggesting the region may be weakly heterotrophic in the summer season, consistent with highly supersaturated fCO_2 in the surface waters of the region (Figure 5c).

These estimates of NCP include uncertainties associated with the analytical determination of TCO_2 concentrations as well as the assumptions regarding winter TCO_2 concentrations. Vertical transport processes that may influence mixed-layer TCO_2 have not been explicitly accounted for, although it is assumed the integration to 100 m accounts for deeper mixing (e.g., Sweeney et al., 2000). In addition, both $CaCO_3$ precipitation/dissolution and the air-sea exchange of CO_2 are not explicitly included in the seasonal deficit approach, although the former has been shown to be a negligible process during the period of observation (section 4.3). The mean instantaneous F_{CO2} computed from our shipboard observations was 0.7 ± 0.9 mmol C m^{-2} day^{-1}. If this mean flux were to persist since 1 November (defined as the beginning of the productive season), then this would lead to an additional $nTCO_2$ concentration of 0.4 μmol/kg in the upper 100 m from the air-sea exchange of CO_2, which is small (<2%), relative to the integrated deficits.

The onset of biological activity in the coastal Antarctic is generally thought to occur when MLDs <40 m (Smith et al., 2000). As most MLD in the open waters of the DP are <40 m, photosynthesis dominates respiration, associated with positive values of NCP. It is likely we observed the beginning of the productive season when NCP rates were relatively low, capturing conditions consistent with the transition from winter to summer. In this period, the biological driver of fCO_2 drawdown has not yet fully compensated for the increased winter fCO_2 due to remineralization (and small seasonal warming of surface waters); thus, surface waters remain supersaturated in fCO_2 despite the positive NCP (i.e., autotrophic conditions). Similarly, dissolved oxygen concentration in AASW within the open waters of the DP was still slightly undersaturated (~1–12%) during the period of observation, suggesting the autotrophic community has not yet fully compensated for loss of dissolved oxygen during the predominating winter heterotrophy. The continuation of summer surface productivity beyond the period of shipboard observation is supported by satellite Chl *a* and discussed in more detail below.

Table 3
The Total Deficit in Surface TCO_2 (ΔTCO_2^{total}; μmol/kg), With Contributions From Seasonal Sea Ice Melt ($\Delta TCO_2^{salinity}$; μmol/kg) and Biological Processes and CO_2 Gas Exchange ($\Delta TCO_2^{bio+gas}$; μmol/kg) and Estimates of Net Community Production (NCP; mmol C m^{-2} day^{-1}) for Each Region During Observations

Variable	DP1	DP2	DP3	WT	ET
ΔTCO_2^{total}	8.2	9.5	19.6	−0.9	3.4
$\Delta TCO_2^{salinity}$	3.5	3.6	12.6	2.3	3.0
$\Delta TCO_2^{bio+gas}$	4.7	5.9	7.0	−3.2	0.4
NCP	12.7	12.9	14.1	−1.5	4.5

The negative NCP that was observed near the TIS may be fueled by the remineralization of allochthonous organic material, which can include production remaining from previous years, assuming the particulate and dissolved organic carbon is labile or semilabile. Upwelling and mixing of TCO_2-rich waters could also be associated with accumulated signals of biological remineralization (rather than the accumulation of organic matter) from distant sources. The MLDs near the western end of the TIS were relatively deep, reaching over 300 m in certain areas, extending well below the depth of our definition for winter TCO_2 concentration and seasonal integration (100 m). This deep mixing could entrain TCO_2-rich

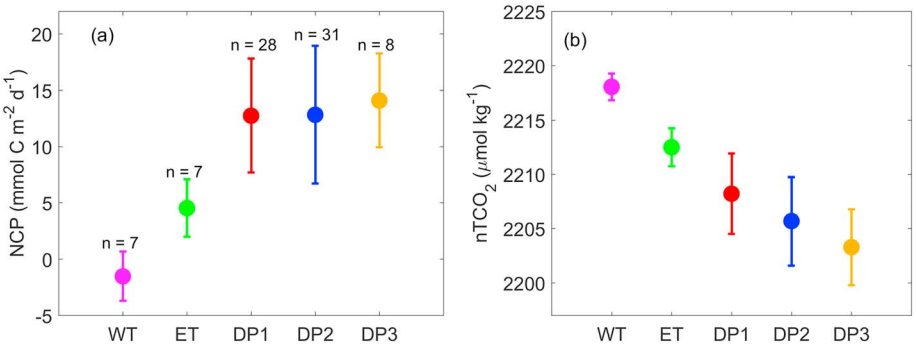

Figure 10. Mean (a) NCP (mmol C m^{-2} day^{-1}) and (b) $nTCO_2$ (μmol/kg) in the mixed layer for each region. Error bars represent the standard deviation.

subsurface water into the summer mixed layer; if these deeper waters have sufficiently high TCO_2 concentrations (from the remineralization of organic matter over timescales that exceed a season), the resulting deficit would indicate net heterotrophic conditions. Finally, since the ice-covered waters near the TIS appear to be significantly less productive than those in the ice-free Dalton Polynya (inferred from the degree of fCO_2 undersaturation), these early summer observations may represent pre-bloom conditions in the TIS perhaps due in part to light limitation associated with sea ice coverage. If the observations had been made later in the season, it is possible that greater surface TCO_2 depletions in a more open TIS region would result in positive NCP (i.e., net autotrophy), similar to conditions observed in the ice-free regions of the adjacent Dalton Polynya. This potential bias due to the timing of observations with respect to ice melt and the onset of open water biological production will be discussed in more detail in the next section.

5.2. Interannual Variability

Coastal shelf waters are known to exhibit significant variability that is difficult to diagnose with shipboard observations (Kaufman et al., 2014; Roden et al., 2013). Fortunately, satellite remote sensing products allow this variability to be assessed over seasonal and interannual timescales in regions where direct biogeochemical observations do not exist. Surface Chl *a* concentrations and sea ice coverage can serve as proxies to assess the variability in biological productivity and the physical environment, respectively, allowing long-term trends in regions with sparse in-situ observations to be evaluated.

Climatological estimates of Chl *a* (mg/m^3) and percent sea ice coverage (%) between 1997 and 2017 (Figure 11) reveal significant interannual variability in the Dalton Polynya. The average seasonal cycle of Chl *a* indicates that the onset of productive season can begin as early as October, when light returns in the austral spring, and suggests that the productive season was underway at the time of observations in early summer. Maximum concentrations of Chl *a* typically peak in January, with an average maximum concentration of 2 mg/m^3 when sea ice coverage is below 50%. In winter (between May and October), there is little and/or nondetectable surface Chl *a* and sea ice coverage is on the order of 70%. Sea ice retreat typically begins in November.

In contrast to the long-term average Chl *a* concentration, the 2014/2015 surface Chl *a* concentrations remained relatively low until February, roughly 1 month after then end of the voyage (black line; Figure 11a). Assuming that Chl *a* can be considered as reliable proxy for biomass, it is likely that increased fCO_2 undersaturation coincided with maximum surface Chl *a* concentrations due to biological drawdown by photosynthesis. During the period of observations in early January, areas of the Dalton Polynya exhibited fCO_2 supersaturation and low surface Chl *a* concentrations. Thus, during the 2014/2015 season, our sampling preceded the height of the open-water productive season, and we observed the early spring-to-summer transition when the surface waters were still supersaturated with respect to atmospheric CO_2. If the growing season persisted through March of the sampling year, as the satellite record suggests, it is likely that the open surface waters would have become undersaturated in the region as a whole and may have transitioned to a sink for atmospheric CO_2 in the late summer and early autumn seasons. This suggests that our seasonal estimates of NCP in the Dalton Polynya may be underestimated, and these values cannot be extrapolated over

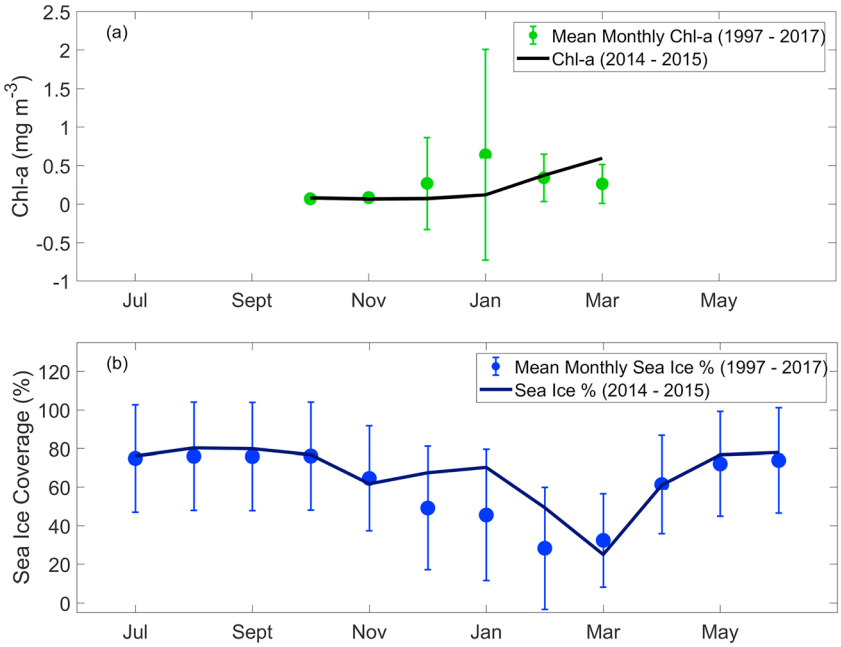

Figure 11. Satellite record of mean monthly (a) surface Chl *a* concentration (mg/m^3) from SeaWiFS (July 1997–June 2002) and MODIS-Aqua (July 2002–June 2017) and (b) percent sea ice coverage (%) from NSIDC (July 1997–June 2017) in the Dalton Polynya. Error bars represent the monthly standard deviations. The black line in each represents the Chl *a* or percent sea ice coverage between July 2014 and June 2015. The absence of points and black line in (a) represents no data.

longer time scales. Similarly, as sea ice coverage near the TIS continued to decline in February, the region may also have transitioned to net autotrophic conditions.

In addition to the role of sea ice in light limitation, sea ice provides a source of dissolved iron to the surface waters during the seasonal melt (Lannuzel et al., 2007), which may stimulate biological productivity (e.g., Sedwick & Ditullio, 1997). During the 2014/2015 season, the onset of sea ice melt in October is in line with the long-term mean (Figure 11b). However, there was an increase in sea ice coverage in December and January, resulting in a greater degree of coverage than the long-term average. This late season sea ice growth would have impeded light penetration, limiting biological productivity and may have restricted the delivery of iron to the surface waters via sea ice melt in early summer.

5.3. Comparison of the Dalton Polynya With Other Coastal Antarctic Systems

Coastal polynyas range widely in their physical icescapes, formation mechanisms, seasonal sea ice dynamics, and wind and current regimes, which ultimately influence spring and summer biological production and CO_2 system properties (e.g., Arrigo et al., 2015). Of the 13 major Antarctic coastal polynyas identified by Nihashi and Ohshima (2015) and Ohshima et al. (2016), the Dalton Polynya ranks eleventh in terms of average wintertime polynya area (3.7 $\pm$ 2.0 10^3 km^2/year with daily standard deviation) and twelfth in terms of its mean annual sea ice production (31 $\pm$ 3 km^3/year) between 2003 and 2011.

The Dalton Polynya has a substantially lower seasonal NCP and summer air-sea CO_2 flux than the majority of observed coastal polynyas and bays in the East Antarctic (Table 4). NCP from this study in the Dalton Polynya was similar to values reported in the Mertz Polynya (Adélie and George V Land region of East Antarctica, 143–148°E) in January 2001 and January 2008, before the calving of the Mertz Glacier Tongue (MGT) in 2010 (Sambrotto et al., 2003; Shadwick et al., 2014). Precalving air-sea CO_2 fluxes in the Mertz Polynya were also slightly greater (−15 mmol C m^{-2} day^{-1}) than the instantaneous fluxes in the Dalton Polynya reported here due to larger degrees of surface fCO_2 undersaturation (Shadwick et al., 2014). However, NCP and air-sea CO_2 exchange rates in the Dalton Polynya stand in contrast to rates from the postcalving configuration of the Mertz Polynya. The MGT calving event substantially reduced Mertz Polynya size and sea ice production in the subsequent years (Nihashi & Ohshima, 2015; Tamura et al., 2012), yet postcalving deficits in mixed-layer TCO_2 concentrations and the rates of NCP and air-to-sea flux of CO_2 in the Mertz

Table 4
Estimates of Net Community Production (NCP) and Air-Sea CO_2 Exchange From Coastal Regions in East Antarctica

Region	Location	NCP	Air-Sea CO_2 Exchange	Year	Reference
Dalton Polynya	66.5 °S 120 °E	10 – 20	−1 to 5	2015	This study
Mertz Polynya	66.5 °S 145 °E	26 – 70	−30 to −5	2013	Shadwick et al. (2017)
		35 – 76		2012	Shadwick et al. (2017)
		25 – 78		2011	Shadwick et al. (2017)
		13 – 27	−15	2008	Sambrotto et al. (2003)
		11 – 19		2001	Shadwick et al. (2014)
Terra Nova Bay, Ross Sea	68.5 °S 75 °E	425 ± 204		2013	DeJong et al. (2017)
			−72 ± 32	2013	DeJong & Dunbar (2017)
Prydz Bay	75.0 °S 165 °E	15 ± 3	−15 to 2	2011	Roden et al. (2013)
			−28.4	1995	Gibson & Trull (1999)
			−37.2	1994	Gibson & Trull (1999)

Note. All units are mmol C m^{-2} day^{-1}.

Polynya dramatically increased in following summers (Shadwick et al., 2017). These corresponding impacts to the CO_2 system have been primarily attributed to an enhancement in biological production as a result of large increases in sea ice meltwater, potentially delivering a source of dissolved iron to the mixed layers (Shadwick et al., 2013). A recent analysis by Moreau et al. (2019) concluded that a larger volume of sea ice meltwater in the Mertz Polynya and neighboring Ninnis Polynya best explained their enhanced biological productivities relative to the Dalton Polynya. The calving of the MGT in the Mertz Polynya set up an interesting natural experiment to assess how changes to the Antarctic icescape impact polynya productivity. As the Dalton Polynya is sustained by the Dalton Iceberg Tongue to the east, a natural calving or shift in the sea ice regime near the Dalton Polynya could potentially lead to changes in the CO_2 system as similarly experienced in the Mertz Polynya system.

NCP and FCO_2 are significantly smaller in the Dalton Polynya than continental shelf waters of the Ross Sea, where annual rates of primary production can reach up to 180 g C m^{-2} $year^{-1}$, among the most productive in the Southern Ocean (Arrigo, van Dijken, & Bushinsky, 2008; Smith & Gordon, 1997). Rates of seasonal NCP exhibit a large range of variability in space and time (Peloquin & Smith, 2007; Smith et al., 2006), though they are several times greater than those observed in the Dalton Polynya (Table 4). In the Terra Nova Bay (TNB) polynya in the western Ross Sea (163–167°E), late summer NCP is an order of magnitude larger than the Dalton polynya at roughly 425 mmol C m^{-2} day^{-1} (Table 4; DeJong et al., 2017). Biological production in TNB is typically dominated by diatoms in summer when stratification is stronger and mixed layers are shallower (Arrigo et al., 2000; Tortell et al., 2011), in contrast to the *Phaeocystis antarctica* communities in the Dalton Polynya (Moreau et al., 2019). Polynya formation in TNB is primarily driven by intense offshore katabatic winds (Bromwich & Kurtz, 1984) that prevent a consolidated sea ice pack from forming in the lee of the Drygalski Ice Tongue, with wind speeds often ranging between 10 and 30 m/s (Bromwich, 1989). DeJong et al. (2017) hypothesize these katabatic winds create ideal conditions for the formation of Langmuir circulation cells that encourage frazil ice formation, concentrate algal biomass in the surface, and potentially introduce micronutrient- (e.g., iron-) rich subsurface waters to boost productivity in late summer. The coupling between enhanced late season primary production and the corresponding undersaturation of surface fCO_2 and strong wind speeds results in extremely high CO_2 uptake rates in TNB surface waters (−75 ± 32 mmol C m^{-2} day^{-1}; Table 4). An analysis of environmental controls on coastal Antarctic productivity by Arrigo et al. (2015) revealed that continental shelf width plays an important role in controlling hot spots of productivity. Wider continental shelves, such as in TNB in the Ross Sea, increase the contact time of bottom waters with iron-rich sediments. Advection of iron-rich subsurface waters to the upper sunlit layers could play a role in driving the late summer TNB productivity (DeJong et al., 2017). This mechanism of iron delivery is less likely on the narrower continental shelf waters in the Dalton Polynya.

In Prydz Bay, located in the Indian Ocean sector of the Antarctic (70–80°E) , NCP rates on the order of 15 ± 3 mmol C m^{-2} day^{-1} (1.8 ± 0.4 mol C/m^2 over a 4-month period) have been reported (Roden et al., 2013). Seasonal deficits in mixed-layer TCO_2 were attributed to a combination of sea ice melt and

biological production (Roden et al., 2013), similar to the drivers of TCO_2 depletion in the Dalton Polynya, resulting in low surface water fCO_2 and an air-to-sea flux of CO_2. Recent studies in Prydz Bay propose that glacial meltwater from the nearby Amery Ice Shelf may bring a large, bioavailable source of dissolved iron from marine-accredited ice beneath the ice shelf, locally enhancing primary productivity (Herraiz-Borreguero et al., 2016). In contrast to the glacial meltwaters introduced by the intrusions of mCDW beneath the TIS and MUIS (warm-regime) to Dalton Polynya, the glacial meltwaters introduced into Prydz Bay are the result of intrusions of cold Dense Shelf Water beneath the Amery Ice Shelf (cold regime; Silvano et al., 2016). The resulting outflow of supercooled ISW can entrain subglacial dissolved iron into the marine ice layer beneath the ice shelf and, upon basal melting, can deliver dissolved iron onto the continental shelf in concentrations up to 4 orders of magnitude higher than typical Southern Ocean waters (Herraiz-Borreguero et al., 2016). In the analysis by Arrigo et al. (2015), the input of basal meltwater by nearby ice shelves can explain almost 60% of the variance in mean Chl *a* concentrations in Antarctic polynyas. The ongoing input of glacial meltwater from the basal melting of the TIS and MUIS may drive future changes to the biological productivity and carbonate chemistry in the adjacent Dalton Polynya waters.

6. Conclusions

New shipboard observations from the Dalton Polynya were used to assess the biological and physical controls on the CO_2 system during the early summer season between December 2014 and January 2015. Profiles of TCO_2 concentration allowed the seasonal NCP to be estimated. The Dalton Polynya is found to be net autotrophic in ice-free areas, though the rates are lower than those observed elsewhere in the East Antarctic. The surface waters near the Totten Ice Shelf show relatively little TCO_2 drawdown, likely due to the ice coverage impeding light penetration to support photosynthesis. NCP near the TIS suggest weakly heterotrophic conditions, with a surplus of organic matter to fuel remineralization potentially coming from the TCO_2-rich winter water during deep mixing. Because polynyas are open or have reduced sea ice cover year-round, they are often thought of as areas of intense biological production leading to enhanced air-sea CO_2 exchange and uptake of atmospheric CO_2. The observations presented here provide an alternative view of Dalton Polynya, with midsummer outgassing of CO_2 to the atmosphere. However, satellite derived Chl *a* concentrations suggest that late-summer productivity increased in parallel with declining sea ice coverage after the completion of the voyage. Long-term remote sensing data indicate interannual variability in surface productivity in the Dalton Polynya and neighboring areas is significant. Improved understanding of CO_2 system dynamics in the coastal Southern Ocean will require more observations to accurately assess the status of these systems as CO_2 sources or sinks.

Acknowledgments
We thank the science party, captain, and crew that participated on the *RV Aurora Australis* AU1402 voyage. This work was supported by the Australian Government's Cooperative Research Centre Program, through the Antarctic Climate & Ecosystems Cooperative Research Centre (ACE CRC), and the Integrated Marine Observing System Ship of Opportunity Program. Mar C. Arroyo is supported by the Graduate Research Fellowship Program (GRFP) through the U.S. National Science Foundation and by the Rebecca Dickhut Endowment through the Virginia Institute of Marine Science. We thank K. Berry, E. van Ooijen, and A. Passmore for collection and analysis of CO_2 system data, S. Rintoul and M. Rosenberg for CTD data, and the CSIRO Hydrochemistry group for the analysis of dissolved oxygen and nutrients. We acknowledge the use of public data products: NCEP/NCAR Reanalysis Derived data provided by NOAA/OAR/ESRL PSD (http://www.esrl.noaa.gov.psd) for wind speed data, NASA OceanColor (http://oceancolor.gsdc.nasa.gov) for satellite chlorophyll measurements, and the National Snow and Ice Data Center (http://nsdic.org) for sea ice coverage. The underway fCO_2 data are publicly available through the Integrated Marine Observing System and the Australian Ocean Data Network (http://aodn.org.au). This paper is Contribution No. 3821 of the Virginia Institute of Marine Science, College of William & Mary.

References

Arrigo, K. R., DiTullio, G. R., Dunbar, R. B., Robinson, D. H., VanWoert, M., Worthen, D. L., & Lizotte, M. P. (2000). Phytoplankton taxonomic variability in nutrient utilization and primary production in the Ross Sea. *Journal of Geophysical Research*, *105*(C4), 8827–8846. https://doi.org/10.1029/1998jc000289

Arrigo, K. R., & van Dijken, G. L. (2003). Phytoplankton dynamics within 37 Antarctic coastal polynya systems. *Journal of Geophysical Research*, *108*(C8), 3271. https://doi.org/10.1029/2002jc001739

Arrigo, K. R., van Dijken, G. L., & Bushinsky, S. (2008). Primary production in the Southern Ocean, 1997–2006. *Journal of Geophysical Research*, *113*, C08004. https://doi.org/10.1029/2007JC004551

Arrigo, K. R., van Dijken, G. L., & Long, M. (2008). Coastal Southern Ocean: A strong anthropogenic CO_2 sink. *Geophysical Research Letters*, *35*, L21602. https://doi.org/10.1029/2008GL035624

Arrigo, K. R., van Dijken, G. L., & Strong, A. L. (2015). Environmental controls of marine productivity hot spots around Antarctica. *Journal of Geophysical Research: Oceans*, *120*, 5545–5565. https://doi.org/10.1002/2015JC010888

Bates, N. R., Hansell, D. A., Carlson, C. A., & Gordon, L. I. (1998). Distribution of CO_2 species, estimates of net community production, and air-sea CO_2 exchange in the Ross Sea polynya. *Journal of Geophysical Research*, *103*(C2), 2883–2896. https://doi.org/10.1029/97jc02473

Broecker, W. S., & Peng, T.-H. (1974). Gas exchange rates between air and sea. *Tellus*, *26*(1–2), 21–35. https://doi.org/10.3402/tellusa.v26i1-2.9733

Bromwich, D. H. (1989). An extraordinary katabatic wind regime at Terra Nova Bay, Antarctica. *Monthly Weather Review*, *117*(3), 688–695. https://doi.org/10.1175/1520-0493(1989)117<0688:aekwra>2.0.co;2

Bromwich, D. H., & Kurtz, D. D. (1984). Katabatic wind forcing of the Terra Nova Bay polynya. *Journal of Geophysical Research*, *89*(C3), 3561–3572. https://doi.org/10.1029/JC089iC03p03561

Carvalho, F., Kohut, J., Oliver, M. J., & Schofield, O. (2017). Defining the ecologically relevant mixed-layer depth for Antarctica's coastal seas. *Geophysical Research Letters*, *44*, 338–345. https://doi.org/10.1002/2016GL071205

DeJong, H. B., & Dunbar, R. B. (2017). Air-sea CO_2 exchange in the Ross Sea, Antarctica. *Journal of Geophysical Research: Oceans*, *122*, 8167–8181. https://doi.org/10.1002/2017JC012853

DeJong, H. B., Dunbar, R. B., Koweek, D. A., Mucciarone, D. A., Bercovici, S. K., & Hansell, D. A. (2017). Net community production and carbon export during the late summer in the Ross Sea, Antarctica. *Global Biogeochemical Cycles*, *31*, 473–491. https://doi.org/10.1002/2016GB005417

DeJong, H. B., Dunbar, R. B., Mucciarone, D., & Koweek, D. A. (2015). Carbonate saturation state of surface waters in the Ross Sea and Southern Ocean: Controls and implications for the onset of aragonite undersaturation. *Biogeosciences*, *12*(23), 6881–6896. https://doi.org/10.5194/bg-12-6881-2015

Dickson, A. G., & Millero, F. J. (1987). A comparison of the equilibrium constants for the dissociation of carbonic acid in seawater media. *Deep Sea Research Part A, Oceanographic Research Papers*, *34*(10), 1733–1743. https://doi.org/10.1016/0198-0149(87)90021-5

Dickson, A. G., Sabine, C. L., & Christian, J. R. (Eds) (2007). *Guide to best practices for ocean CO_2 measurements*, *PICES Special Publication 3*, (p. 191). Sydney, B.C., Canada: North Pacific Marine Science Organization.

Dieckmann, G. S., Nehrke, G., Papadimitriou, S., Göttlicher, J., Steininger, R., Kennedy, H., et al. (2008). Calcium carbonate as ikaite crystals in Antarctic sea ice. *Geophysical Research Letters*, *35*, L08501. https://doi.org/10.1029/2008GL033540

Edson, J. B., Fairall, C. W., Bariteau, L., Zappa, C. J., Cifuentes-Lorenzen, A., McGillis, W. R., et al. (2011). Direct covariance measurement of CO_2 gas transfer velocity during the 2008 Southern Ocean Gas Exchange Experiment: Wind speed dependency. *Journal of Geophysical Research*, *116*, C00F10. https://doi.org/10.1029/2011JC007022

Evans, W., Mathis, J. T., Cross, J. N., Bates, N. R., Frey, K. E., Else, B. G. T., et al. (2015). Sea-air CO_2 exchange in the western Arctic coastal ocean. *Global Biogeochemical Cycles*, *29*, 1190-1209. https://doi.org/10.1002/2015gb005153

Eveleth, R., Cassar, N., Sherrell, R. M., Ducklow, H., Meredith, M. P., Venables, H. J., et al. (2017). Ice melt influence on summertime net community production along the Western Antarctic Peninsula. *Deep-Sea Research Part II: Topical Studies in Oceanography*, *139*, 89–102. https://doi.org/10.1016/j.dsr2.2016.07.016

Gerringa, L. J., Alderkamp, A. C., Laan, P., Thuróczy, C. E., de Baar, H. J., Mills, M. M., et al. (2012). Iron from melting glaciers fuels the phytoplankton blooms in Amundsen Sea (Southern Ocean): Iron biogeochemistry. *Deep-Sea Research Part II: Topical Studies in Oceanography*, *71-76*, 16–31. https://doi.org/10.1016/j.dsr2.2012.03.007

Gibson, J. A. E., & Trull, T. W. (1999). Annual cycle of fCO2 under sea-ice and in open water in Prydz Bay, East Antarctica. *Marine Chemistry*, *66*(3–4), 187–200. https://doi.org/10.1016/s0304-4203(99)00040-7

Grasshoff, K., Kremling, K., & Ehrhardt, M. (2007). *Methods of seawater analysis: Third edition. Completely Revised and Extended Edition*. Weinheim, Germany: Wiley-VCH. https://doi.org/10.1002/9783527613984

Greenbaum, J. S., Blankenship, D. D., Young, D. A., Richter, T. G., Roberts, J. L., Aitken, A. R. A., et al. (2015). Ocean access to a cavity beneath Totten Glacier in East Antarctica. *Nature Geoscience*, *8*(4), 294–298. https://doi.org/10.1038/ngeo2388

Greene, C. A., Blankenship, D. D., Gwyther, D. E., Silvano, A., & van Wijk, E. (2017). Wind causes Totten Ice Shelf melt and acceleration. *Science Advances*, *3*(11), e1701681. https://doi.org/10.1126/sciadv.1701681

Gruber, N., Gloor, M., Mikaloff Fletcher, S. E., Doney, S. C., Dutkiewicz, S., Follows, M. J., et al. (2009). Oceanic sources, sinks, and transport of atmospheric CO_2. *Global Biogeochemical Cycles*, *23*, GB1005. https://doi.org/10.1029/2008GB003349

Herraiz-Borreguero, L., Lannuzel, D., van der Merwe, P., Treverrow, A., & Pedro, J. B. (2016). Large flux of iron from the Amery Ice Shelf marine ice to Prydz Bay, East Antarctica. *Journal of Geophysical Research: Oceans*, *121*, 6009–6020. https://doi.org/10.1002/2016JC011687

Ho, D. T., Law, C. S., Smith, M. J., Schlosser, P., Harvey, M., & Hill, P. (2006). Measurements of air-sea gas exchange at high wind speeds in the Southern Ocean: Implications for global parameterizations. *Geophysical Research Letters*, *33*, L16611. https://doi.org/10.1029/2006GL026817

Hood, E. M., Sabine, C. L., & Sloyan, B. M. (2010). The GO-SHIP Repeat Hydrography Manual: A collection of expert reports and guidelines. IOCCP Report 14, ICPO Publication Series 134. https://doi.org/10.21125/inted.2016.1955

Jones, E. M., Bakker, D. C. E., Venables, H. J., Whitehouse, M. J., Korb, R. E., & Watson, A. J. (2010). Rapid changes in surface water carbonate chemistry during Antarctic sea ice melt. *Tellus Series B: Chemical and Physical Meteorology*, *62*(5), 621–635. https://doi.org/10.1111/j.1600-0889.2010.00496.x

Jones, E. M., Fenton, M., Meredith, M. P., Clargo, N. M., Ossebaar, S., Ducklow, H. W., et al. (2017). Ocean acidification and calcium carbonate saturation states in the coastal zone of the West Antarctic Peninsula. *Deep-Sea Research Part II: Topical Studies in Oceanography*, *139*, 181–194. https://doi.org/10.1016/j.dsr2.2017.01.007

Kalnay, E., Kanamitsu, M., Kistler, R., Collins, W., Deaven, D., Gandin, L., et al. (1996). The NCEP/NCAR 40-year reanalysis project. *Bulletin of the American Meteorological Society*, *77*(3), 437–471. https://doi.org/10.1175/1520-0477(1996)077<0437:TNYRP>2.0.CO;2

Kaufman, D. E., Friedrichs, M. A. M., Smith, W. O., Queste, B. Y., & Heywood, K. J. (2014). Biogeochemical variability in the southern Ross Sea as observed by a glider deployment. *Deep Sea Research Part I: Oceanographic Research Papers*, 92, 93-106. https://doi.org/10.1016/j.dsr.2014.06.011

Khatiwala, S., Primeau, F., & Hall, T. (2009). Reconstruction of the history of anthropogenic CO_2 concentrations in the ocean. *Nature*, *462*(7271), 346–349. https://doi.org/10.1038/nature08526

Lannuzel, D., Schoemann, V., de Jong, J., Tison, J. L., & Chou, L. (2007). Distribution and biogeochemical behaviour of iron in the East Antarctic sea ice. *Marine Chemistry*, *106*(1–2), 18–32. https://doi.org/10.1016/j.marchem.2006.06.010

Legge, O. J., Bakker, D. C. E., Meredith, M. P., Venables, H. J., Brown, P. J., Jones, E. M., & Johnson, M. T. (2017). The seasonal cycle of carbonate system processes in Ryder Bay, West Antarctic Peninsula. *Deep-Sea Research Part II: Topical Studies in Oceanography*, *139*, 167–180. https://doi.org/10.1016/j.dsr2.2016.11.006

Lenton, A., Tilbrook, B., Law, R. M., Bakker, D., Doney, S. C., Gruber, N., et al. (2013). Sea–air CO_2 fluxes in the Southern Ocean for the period 1990–2009. *Biogeosciences*, *10*(6), 4037–4054. https://doi.org/10.5194/bg-10-4037-2013

Li, X., Rignot, E., Morlighem, M., Mouginot, J., & Scheuchl, B. (2015). Grounding line retreat of Totten Glacier, East Antarctica, 1996 to 2013. *Geophysical Research Letters*, *42*, 8049–8056. https://doi.org/10.1002/2015GL065701

Loose, B., Schlosser, P., Perovich, D., Ringelberg, D., Ho, D. T., Takahashi, T., et al. (2011). Gas diffusion through columnar laboratory sea ice: Implications for mixed-layer ventilation of CO_2 in the seasonal ice zone. *Tellus Series B: Chemical and Physical Meteorology*, *63*(1), 23–39. https://doi.org/10.1111/j.1600-0889.2010.00506.x

Massom, R. A., Harris, P. T., Michael, K. J., & Potter, M. J. (1998). The distribution and formative processes of latent-heat polynyas in East Antarctica. *Annals of Glaciology*, *27*(1), 420–426. https://doi.org/10.3189/1998AoG27-1-420-426

McNeil, B. I., Sweeney, C., & Gibson, J. A. E. (2011). Short Note: Natural seasonal variability of aragonite saturation state within two Antarctic coastal ocean sites. *Antarctic Science*, *23*(4), 411–412. https://doi.org/10.1017/s0954102011000204

Mehrbach, C., Culberson, C. H., Hawley, J. E., & Pytkowicx, R. M. (1973). Measurement of the apparent dissociation constants of carbonic acid in seawater at atmospheric pressure. *Limnology and Oceanography*, *18*(6), 897–907. https://doi.org/10.4319/lo.1973.18.6.0897

Mohajerani, Y., Velicogna, I., & Rignot, E. (2018). Mass loss of Totten and Moscow University Glaciers, East Antarctica, using regionally optimized GRACE mascons. *Geophysical Research Letters*, *45*, 7010–7018. https://doi.org/10.1029/2018GL078173

Morales Maqueda, M. A., Willmott, A. J., & Biggs, N. R. T. (2004). Polynya dynamics: A review of observations and modeling. *Reviews of Geophysics*, *42*, RG1004. https://doi.org/10.1029/2002RG000116

Moreau, S., Lannuzel, D., Janssens, J., Arroyo, M. C., Corkill, C., Cougnon, E., et al. (2019). Sea-ice meltwater and circumpolar deep water drive contrasting productivity in three Antarctic polynyas. *Journal of Geophysical Research: Oceans*, *124*, 2943–2968. https://doi.org/10.1029/2019JC015071

Mu, L., Stammerjohn, S. E., Lowry, K. E., & Yager, P. L. (2014). Spatial variability of surface pCO_2 and air-sea CO_2 flux in the Amundsen Sea Polynya, Antarctica. *Elementa: Science of the Anthropocene*, *2*, 000036. https://doi.org/10.12952/journal.elementa.000036

Nihashi, S., & Ohshima, K. I. (2015). Circumpolar mapping of Antarctic coastal polynyas and landfast sea ice: Relationship and variability. *Journal of Climate*, *28*(9), 3650–3670. https://doi.org/10.1175/JCLI-D-14-00369.1

Ohshima, K. I., Nihashi, S., & Iwamoto, K. (2016). Global view of sea-ice production in polynyas and its linkage to dense/bottom water formation. *Geoscience Letters*, *3*(1), 13. https://doi.org/10.1186/s40562-016-0045-4

Orsi, A. H., Johnson, G. C., & Bullister, J. L. (1999). Circulation, mixing, and production of Antarctic Bottom Water. *Progress in Oceanography*, *43*(1), 55–109. https://doi.org/10.1016/S0079-6611(99)00004-X

Peloquin, J. A., & Smith, W. O. Jr. (2007). Phytoplankton blooms in the Ross Sea, Antarctica: Interannual variability in magnitude, temporal patterns, and composition. *Journal of Geophysical Research*, *112*, C08013. https://doi.org/10.1029/2006JC003816

Pierrot, D., Neill, C., Sullivan, K., Castle, R., Wanninkhof, R., Lüger, H., et al. (2009). Recommendations for autonomous underway pCO_2 measuring systems and data-reduction routines. *Deep-Sea Research Part II: Topical Studies in Oceanography*, *56*(8–10), 512–522. https://doi.org/10.1016/j.dsr2.2008.12.005

Rignot, E., Jacobs, S., Mouginot, J., & Scheuchl, B. (2013). Ice-shelf melting around Antarctica. *Science*, *341*(6143), 266–270. https://doi.org/10.1126/science.1235798

Riley, J. P., & Tongudai, M. (1967). The major cation/chlorinity ratios in sea water. *Chemical Geology*, *2*(C), 263–269. https://doi.org/10.1016/0009-2541(67)90026-5

Rintoul, S. R. (1998). On the origin and influence of Adélie land bottom water. In *Ocean, Ice, and Atmosphere: interactins at the Antarctic continental margin*, (Vol. 75, pp. 151–171). Washington, D. C: American Geophysical Union. https://doi.org/10.1029/ar075p0151

Rintoul, S. R., Silvano, A., Pena-Molino, B., van Wijk, E., Rosenberg, M., Greenbaum, J. S., & Blankenship, D. D. (2016). Ocean heat drives rapid basal melt of the Totten Ice Shelf. *Science Advances*, *2*(12), e1601610. https://doi.org/10.1126/sciadv.1601610

Roden, N. P., Shadwick, E. H., Tilbrook, B., & Trull, T. W. (2013). Annual cycle of carbonate chemistry and decadal change in coastal Prydz Bay, East Antarctica. *Marine Chemistry*, *155*, 135–147. https://doi.org/10.1016/j.marchem.2013.06.006

Roden, N. P., Tilbrook, B., Trull, T. W., Virtue, P., & Williams, G. D. (2016). Carbon cycling dynamics in the seasonal sea-ice zone of East Antarctica. *Journal of Geophysical Research: Oceans*, *121*, 8749–8769. https://doi.org/10.1002/2016JC012008

Rosenberg M., & Rinoul, S. R. (2016). Aurora Australis Marine Science Cruise AU1402, Totten and Mertz CTDs and moorings—Oceanographic field measurements and analysis. *Rep*., Hobart, Australia.

Rysgaard, S., Glud, R. N., Lennert, K., Cooper, M., Halden, N., Leakey, R. J. G., et al. (2012). Ikaite crystals in melting sea ice—Implications for pCO2 and pH levels in Arctic surface waters. *The Cryosphere*, *6*(4), 901–908. https://doi.org/10.5194/tc-6-901-2012

Sabine, C. L., Feely, R. A., Gruber, N., Key, R. M., Lee, K., Bullister, J. L., et al. (2004). The oceanic sink for anthropogenic CO_2. *Science*, *305*(5682), 367–371. https://doi.org/10.1126/science.1097403

Sambrotto, R. N., Matsuda, A., Vaillancourt, R., Brown, M., Langdon, C., Jacobs, S. S., & Measures, C. (2003). Summer plankton production and nutrient consumption patterns in the Mertz Glacier Region of East Antarctica. *Deep-Sea Research Part II: Topical Studies in Oceanography*, *50*(8–9), 1393–1414. https://doi.org/10.1016/S0967-0645(03)00076-6

Sedwick, P. N., & Ditullio, G. R. (1997). Regulation of algal blooms in Antarctic shelf waters by the release of iron from melting sea ice. *Geophysical Research Letters*, *24*(20), 2515–2518. https://doi.org/10.1029/97GL02596

Shadwick, E. H., Rintoul, S. R., Tilbrook, B., Williams, G. D., Young, N., Fraser, A. D., et al. (2013). Glacier tongue calving reduced dense water formation and enhanced carbon uptake. *Geophysical Research Letters*, *40*, 904–909. https://doi.org/10.1002/grl.50178

Shadwick, E. H., Tilbrook, B., & Currie, K. I. (2017). Late-summer biogeochemistry in the Mertz Polynya: East Antarctica. *Journal of Geophysical Research: Oceans*, *122*, 7380–7394. https://doi.org/10.1002/2017JC013015

Shadwick, E. H., Tilbrook, B., & Williams, G. D. (2014). Carbonate chemistry in the Mertz Polynya (East Antarctica): Biological and physical modification of dense water outflows and the export of anthropogenic CO_2. *Journal of Geophysical Research: Oceans*, *119*, 1–14. https://doi.org/10.1002/2013JC009286

Silvano, A., Rintoul, S., & Herraiz-Borreguero, L. (2016). Ocean-ice shelf interaction in East Antarctica. *Oceanography*, *29*(4), 130–143. https://doi.org/10.5670/oceanog.2016.105

Silvano, A., Rintoul, S. R., Peña-Molino, B., Hobbs, W. R., van Wijk, E., Aoki, S., et al. (2018). Freshening by glacial meltwater enhances melting of ice shelves and reduces formation of Antarctic Bottom Water. *Science Advances*, *4*(4), eaap9467. https://doi.org/10.1126/sciadv.aap9467

Silvano, A., Rintoul, S. R., Peña-Molino, B., & Williams, G. D. (2017). Distribution of water masses and meltwater on the continental shelf near the Totten and Moscow University ice shelves. *Journal of Geophysical Research: Oceans*, *122*, 2050–2068. https://doi.org/10.1002/2016JC012115

Smith, W. O. Jr., & Gordon, L. I. (1997). Hyperproductivity of the Ross Sea (Antarctica) polynya during austral spring. *Geophysical Research Letters*, *24*(3), 233–236. https://doi.org/10.1029/96GL03926

Smith, W. O. Jr., Shields, A. R., Peloquin, J. A., Catalano, G., Tozzi, S., Dinniman, M. S., & Asper, V. A. (2006). Interannual variations in nutrients, net community production, and biogeochemical cycles in the Ross Sea. *Deep-Sea Research Part II: Topical Studies in Oceanography*, *53*(8–10), 815–833. https://doi.org/10.1016/j.dsr2.2006.02.014

Smith, W. O., Marra, J., Hiscock, M. R., & Barber, R. T. (2000). The seasonal cycle of phytoplankton biomass and primary productivity in the Ross Sea, Antarctica. *Deep Sea Research Part II: Topical Studies in Oceanography*, *47*(15–16), 3119–3140. https://doi.org/10.1016/s0967-0645(00)00061-8

Sweeney, C. (2003). The annual cycle of surface water CO_2 and O_2 in the Ross Sea: A model for gas exchange on the continental shelves of Antarctica. In *Biogeochemistry of the Ross Sea*, (Vol. 78, pp. 295–312). Washington, D. C: American Geophysical Union. https://doi.org/10.1029/078ars19

Sweeney, C., Gloor, E., Jacobson, A. R., Key, R. M., McKinley, G., Sarmiento, J. L., & Wanninkhof, R. (2007). Constraining global air-sea gas exchange for CO_2 with recent bomb ^{14}C measurements. *Global Biogeochemical Cycles*, *21*, GB2015. https://doi.org/10.1029/2006GB002784

Sweeney, C., Hansell, D. A., Carlson, C. A., Codispoti, L. A., Gordon, L. I., Marra, J., et al. (2000). Biogeochemical regimes, net community production and carbon export in the Ross Sea, Antarctica. *Deep-Sea Research Part II: Topical Studies in Oceanography*, *47*(15–16), 3369–3394. https://doi.org/10.1016/S0967-0645(00)00072-2

Takahashi, T., Sutherland, S. C., Wanninkhof, R., Sweeney, C., Feely, R. A., Chipman, D. W., et al. (2009). Climatological mean and decadal change in surface ocean pCO_2, and net sea-air CO_2 flux over the global oceans. *Deep-Sea Research Part II: Topical Studies in Oceanography*, *56*(8–10), 554–577. https://doi.org/10.1016/j.dsr2.2008.12.009

Tamura, T., Williams, G. D., Fraser, A. D., & Ohshima, K. I. (2012). Potential regime shift in decreased sea ice production after the Mertz Glacier calving. *Nature Communications*, *3*(1), 826. https://doi.org/10.1038/ncomms1820

Tortell, P. D., Guéguen, C., Long, M. C., Payne, C. D., Lee, P., & DiTullio, G. R. (2011). Spatial variability and temporal dynamics of surface water pCO_2, ΔO_2/Ar and dimethylsulfide in the Ross Sea, Antarctica. *Deep-Sea Research Part I: Oceanographic Research Papers*, *58*(3), 241–259. https://doi.org/10.1016/j.dsr.2010.12.006

van Heuven, S., Pierrot, D., Rae, J. W. B., Lewis, E., & Wallace, D. W. R. (2011). MATLAB Program Developed for CO_2 System Calculations. ORNL/CDIAC-105b. Oak Ridge, Tennessee: Carbon Dioxide Information Analysis Center, Oak Ridge National Laboratory, U.S. Department of Energy. https://doi.org/10.3334/CDIAC/otg.CO2SYS_MATLAB_v1.1

Wanninkhof, R. (1992). Relationship between wind speed and gas exchange over the ocean. *Journal of Geophysical Research*, *97*(C5), 7373. https://doi.org/10.1029/92JC00188

Wanninkhof, R. (2014). Relationship between wind speed and gas exchange over the ocean revisited. *Limnology and Oceanography: Methods*, *12*, 351–362. https://doi.org/10.4319/lom.2014.12.351

Wanninkhof, R., Sullivan, K. F., & Top, Z. (2004). Air-sea gas transfer in the Southern Ocean. *Journal of Geophysical Research*, *109*, C08S19. https://doi.org/10.1029/2003jc001767

Weiss, R. F. (1974). Carbon dioxide in water and seawater: The solubility of a non-ideal gas. *Marine Chemistry*, *2*(3), 203–215. https://doi.org/10.1016/0304-4203(74)90015-2

Williams, G. D., Bindoff, N. L., Marsland, S. J., & Rintoul, S. R. (2008). Formation and export of dense shelf water from the Adélie depression, East Antarctica. *Journal of Geophysical Research*, *113*, C04039. https://doi.org/10.1029/2007JC004346

Williams, G. D., Meijers, A. J. S., Poole, A., Mathiot, P., Tamura, T., & Klocker, A. (2011). Late winter oceanography off the Sabrina and BANZARE coast (117-128°E), East Antarctica. *Deep-Sea Research Part II: Topical Studies in Oceanography*, *58*(9–10), 1194–1210. https://doi.org/10.1016/j.dsr2.2010.10.035

Yager, P., Sherrell, R., Stammerjohn, S., Ducklow, H., Schofield, O., Ingall, E., et al. (2016). A carbon budget for the Amundsen Sea Polynya, Antarctica: Estimating net community production and export in a highly productive polar ecosystem. *Elementa: Science of the Anthropocene*, *4*, 000140. https://doi.org/10.12952/journal.elementa.000140

Yager, P. L., Wallace, D. W. R., Johnson, K. M., Smith, W. O., Minnett, P. J., & Deming, J. W. (1995). The Northeast Water Polynya as an atmospheric CO_2 sink: A seasonal rectification hypothesis. *Journal of Geophysical Research*, *100*(C3), 4389–4398. https://doi.org/10.1029/94JC01962